Review article **Open Access**

Aziz Genç*, Javier Patarroyo, Jordi Sancho-Parramon, Neus G. Bastús, Victor Puntes and Jordi Arbiol*

Hollow metal nanostructures for enhanced plasmonics: synthesis, local plasmonic properties and applications

DOI 10.1515/nanoph-2016-0124
Received July 5, 2016; revised July 26, 2016; accepted August 1, 2016

Abstract: Metallic nanostructures have received great attention due to their ability to generate surface plasmon resonances, which are collective oscillations of conduction electrons of a material excited by an electromagnetic wave. Plasmonic metal nanostructures are able to localize and manipulate the light at the nanoscale and, therefore, are attractive building blocks for various emerging applications. In particular, hollow nanostructures are promising plasmonic materials as cavities are known to have better plasmonic properties than their solid counterparts thanks to the plasmon hybridization mechanism. The hybridization of the plasmons results in the enhancement of the plasmon fields along with more homogeneous distribution as well as the reduction of localized surface plasmon resonance (LSPR) quenching due to absorption. In this review, we summarize the efforts on the synthesis of hollow metal nanostructures with an emphasis on the galvanic replacement reaction. In the second part of this review, we discuss the advancements on the characterization of plasmonic properties of hollow nanostructures, covering the single nanoparticle experiments, nanoscale characterization via electron energy-loss spectroscopy and modeling and simulation studies. Examples of the applications, i.e. sensing, surface enhanced Raman spectroscopy, photothermal ablation therapy of cancer, drug delivery or catalysis among others, where hollow nanostructures perform better than their solid counterparts, are also evaluated.

Keywords: hollow nanostructures; surface plasmon resonances (SPRs); plasmon hybridization; electron energy-loss spectroscopy (EELS); applications.

***Corresponding authors: Aziz Genç,** Catalan Institute of Nanoscience and Nanotechnology (ICN2), CSIC and The Barcelona Institute of Science and Technology (BIST), Campus UAB, Bellaterra, 08193 Barcelona, Catalonia, Spain; and Department of Metallurgy and Materials Engineering, Faculty of Engineering, Bartin University, 74100 Bartin, Turkey, e-mail: azizgenc@gmail.com; and
Jordi Arbiol, Catalan Institute of Nanoscience and Nanotechnology (ICN2), CSIC and The Barcelona Institute of Science and Technology (BIST), Campus UAB, Bellaterra, 08193 Barcelona, Catalonia, Spain; and ICREA, Pg. Lluís Companys 23, 08010 Barcelona, Catalonia, Spain, e-mail: arbiol@icrea.cat
Javier Patarroyo and Neus G. Bastús: Catalan Institute of Nanoscience and Nanotechnology (ICN2), CSIC and The Barcelona Institute of Science and Technology (BIST), Campus UAB, Bellaterra, 08193 Barcelona, Catalonia, Spain
Jordi Sancho-Parramon: Rudjer Boskovic Institute, Zagreb, Croatia
Victor Puntes: Catalan Institute of Nanoscience and Nanotechnology (ICN2), CSIC and The Barcelona Institute of Science and Technology (BIST), Campus UAB, Bellaterra, 08193 Barcelona, Catalonia, Spain; Vall d'Hebron Institut de Recerca (VHIR), 08035, Barcelona, Catalonia, Spain; and ICREA, Pg. Lluís Companys 23, 08010 Barcelona, Catalonia, Spain

1 Introduction

Research on the metallic nanostructures has been quite intensive over the years thanks to their ability to generate surface plasmon resonances (SPRs), which are collective oscillations of conduction electrons of the metals at the interface with a dielectric media. Plasmon resonances provide the capability of the localization and manipulation of light at nanoscale [1], which makes plasmonic nanostructures attractive building blocks for various novel applications spanning over the fields of biology, physics, chemistry, engineering, and medicine. For instance, they are widely used in sensing, surface enhanced Raman spectroscopy (SERS), plasmon-enhanced solar cells, photodetectors, drug delivery and cancer therapy as well as nanolasers, invisibility cloaks, and quantum computing [2–8].

In general, silver can be regarded as the most important material in the field of plasmonics with the ability to generate plasmon resonances between 300 and 1200 nm

©2016, Aziz Genç, Jordi Arbiol et al., published by De Gruyter.
This work is licensed under the Creative Commons Attribution-NonCommercial-NoDerivatives 3.0 License.
Brought to you by | Hospital Universitari Vall d'Hebron
Authenticated
Download Date | 3/7/19 12:30 PM

with much higher quality factors than the other noble metals such as Au and Cu [9]. It is due to the fact that interband transitions, where conduction band electrons are excited to higher energy levels, take place at much higher frequencies than the plasmon resonances of Ag. For the case of Au and Cu nanostructures, the onset of interband transitions partially overlaps with the plasmon resonances, causing a decrease in the plasmon intensity [10–12]. However, the stability and biocompatibility of Ag nanostructures limit their use in many bio-related applications. It would be appealing if a material could combine features of both Au and Ag, i.e. a material as stable as Au that can generate plasmon fields as intense as Ag. Hollow AuAg nanostructures come into prominence as a potential solution for such combination of features as cavities are known to have better plasmonic properties than their solid counterparts thanks to a mechanism called plasmon hybridization [13]. Mahmoud et al. [14] revealed by discrete dipole approximation (DDA) simulations that Au nanoframes can generate plasmonic fields whose intensities are comparable to those of Ag nanocubes. Thanks to the enhanced plasmonic fields, hollow metal nanostructures have been used in many applications such as sensing, SERS, photo thermal ablation (PTA) of cancer, drug delivery, and catalysis over the years with performances better than their solid counter parts, which is reviewed in detail in Section 4.

Hollow nanostructures with controlled hollow interior and shell thickness represent a class of important nanostructured materials due to their above-mentioned outstanding properties and widespread potential applications [15]. The possibility to develop novel hollow nanostructures toward many desired applications relies on the optimization of their performance, which is adjusted by the fine tuning of their properties and is ultimately determined by the control of their morphological and structural parameters. These challenging requirements can be achieved chemically, by the development of new and robust synthetic processes leading to the reproducible, scalable, and cost-effective production of hollow nanostructures with a high uniformity and well-controlled morphology, structure, and surface chemistry. In Section 2, we present a comprehensive summary on the synthesis of hollow nanostructures via templating approaches [16] and galvanic replacement reactions (GRRs) [17–19] with an emphasis on the latter technique.

As we present the plasmon hydridization mechanism and plasmon fields generated due to the hybridization as the main reason of the enhanced plasmonic properties of hollow nanostructures, we believe it should be presented here in more detail. The plasmon hybridization mechanism, developed by Prodan et al. [13], is a model used to explain the plasmon resonances of nanostructures with complex nanostructures as they are generated due to the interaction or "hybridization" of plasmon excitations of simpler geometries. This principle has opened the way to rational designs of complex nanostructures with desired plasmonic properties by a simple approach [20]. The most common and simplistic case of plasmon hybridization is a dimer of two closely located nanostructures [21], and the term is widely used to explain the interaction between two solid nanostructures or the interaction between the nanostructure and the environment, i.e. the substrate [22–35]. In this review, we will focus on the plasmon hybridization in hollow nanostructures [13, 20, 36–40].

The hybridization model for a nanoshell is schematically shown in Figure 1A [13], where the energy-level diagram describing the mechanism of excitation of the hybridized plasmon resonances in metal nanoshells by the interaction between the sphere surface (ω_{sp}) and inner cavity (ω_{c}) surface plasmons is presented. As shown in the hybridization model in Figure 1A, two fundamental dipolar modes of a void/shell nanoparticle system can be considered as they emerged by the hybridization of dipolar modes of a metallic sphere and a dielectric void in a metallic substrate. Hybridization results in the splitting and shifting of these plasmon resonances, as a result, an anti-symmetrically coupled anti-bonding mode (ω_{+}) and symmetrically coupled bonding mode (ω_{-}) are generated in the metallic shell. Validity of this model is proven by quantum mechanical calculations and finite-difference time-domain (FDTD) simulations [36, 40, 41]. The plasmon hybridization model can explain the interactions between the plasmon resonances of more complex systems such as double-shell metallic nanoparticles [13]. More recently, it has been implemented to explain quantum plasmonics in a complex system, so-called "nanomatryushka" [42].

It is well known that the localized surface plasmon resonance (LSPR) properties of the metallic nanostructures are highly affected by parameters like size, shape, and composition of the nanostructures and the environment [43, 44]. Accordingly, many different nanostructures have been investigated so far [45]. In order to design nanostructures with desired plasmonic features, one must fully apprehend and locate the distribution of plasmon resonances with the highest possible spatial accuracy. Techniques such as UV-Vis-NIR spectroscopy, dark field microscopy, and near-field scanning optical microscopy are commonly used to characterize the plasmonic properties of metallic nanostructures; however, their spatial resolution limitations restrain the complete characterization of local optical features within the individual nanostructures.

Brought to you by | Hospital Universitari Vall d'Hebron
Authenticated
Download Date | 3/7/19 12:30 PM

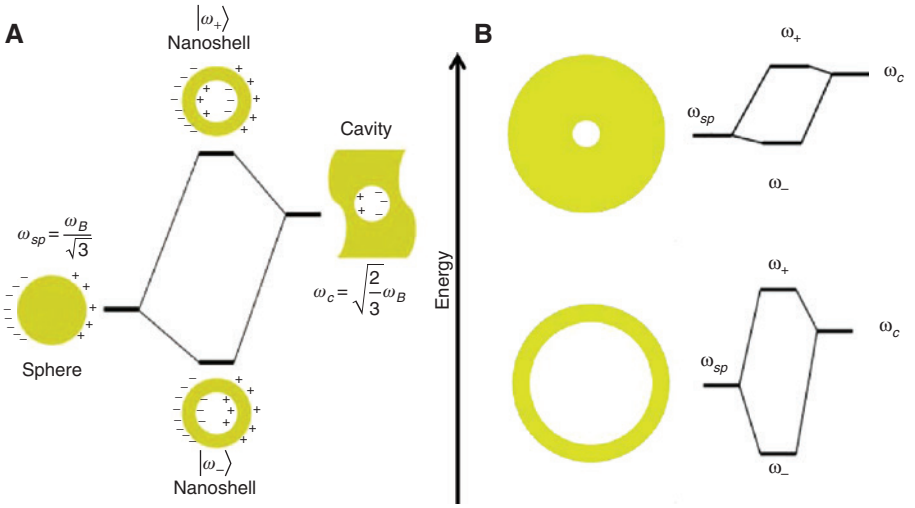

Figure 1: Plasmon hybridization mechanism. (A) Schematic energy-level diagram illustrating the plasmon hybridization mechanism in metal nanoshells as a result of the interaction between the sphere (ω_{sp}) and cavity (ω_c) plasmons. Anti-symmetrically coupled, anti-bonding, mode (ω_+) and symmetrically coupled, bonding, mode (ω_-) are shown (reproduced with permission from Ref. [13], copyright 2003 American Association for the Advancement of Science). (B) Extent of the hybridization for thick (upper) and thin (lower) metallic shells revealing that the hybridization is much more significant for the thin metallic shell (adapted with permission from Ref. [39], copyright 2011 Cambridge University Press).

To overcome this challenge, electron energy-loss spectroscopy (EELS) in a scanning transmission electron microscope (STEM) equipped with a monochromator is a very promising characterization tool with its high spatial (sub-nanometer scale) and high energy (below 0.2 eV) resolutions [46, 47]. Along with the experimental techniques such as EELS, simulation studies by techniques such as DDA and boundary element method (BEM) are known to provide comprehensive information about the ultralocal plasmonic properties of the nanostructures [48–53]. In this review, we focus on the characterization of the ultralocal plasmonic properties of hollow nanostructures at the sub-nanoparticle (nano-) scale, where we cover the efforts starting from the early single nanoparticle experiments, recent EELS, and simulation studies.

In this review, we summarize the efforts on the synthesis of hollow metal nanostructures with an emphasis on the GRR. We discuss the advancements on the characterization of local plasmonic properties of hollow nanostructures and examples of the applications, i.e. sensing, SERS, PTA of cancer, drug delivery or catalysis, where hollow nanostructures perform better than their solid counterparts.

2 Synthesis of hollow nanostructures

The most popular approach for the synthesis of hollow nanoparticles involves coating of the desired materials onto sacrificial templates [16]. These templating strategies, based on the coating of pre-fabricated (hard or soft) templates with a layer of a shell material, are conceptually the simplest one. By the use of hard templates, hollow nanocrystals (NCs) are obtained after a selective removal process, which typically involves processes of dissolution, chemical etching, thermal decomposition, or calcination. Oppositely, in the soft-templating approaches no template removal procedure is required. In both of these approaches, the void size and the shape of the hollow structure are determined by the nature of the template while the morphology and composition of the shell (material, thickness and porosity) is mainly defined in the coating and removal processes. As a result, a wide variety of hollow NCs with different sizes, shapes, composition, and structures have been produced, using hard templates, such as polymers (polystyrene [54, 55], formaldehyde resin [56, 57], and poly(methyl)methacrylate [58], silica [59, 60] and carbon particles [61]), or soft ones, such as emulsion block copolymer micelles [62], and even gas bubbles [63]. For a comprehensive and up-to-date review on templating approaches see Ref. [16].

Inspite of its simplicity and high versatility this conventional templating strategy presents some important limitations, associated with the difficulty of their fabrication in large quantities. This problem together with the complexity of the surface coating processes needed for the shell formation, which usually involves tedious surface functionalization procedures, and the use of toxic etchants or solvents in the removal processes, restricts its

Brought to you by | Hospital Universitari Vall d'Hebron
Authenticated
Download Date | 3/7/19 12:30 PM

synthetic reproducibility and ultimately their applicability. In this regard, the direct synthesis of hollow nanostructures without the need of additional templates are significantly advantageous due to its reduced production cost, simplified synthetic procedure, high reproducibility, great control over particle morphology and uniformity, and an easy scale up.

The chemical transformations of pre-formed solid nanostructures, principally via galvanic replacement and nanoscale Kirkendall effect, represent extremely powerful and versatile strategies to generate complex hollow nanostructures with tunable and well-controlled properties that are often not attainable by other methods. The GRR is one of the most efficient strategies to combine different metals in a single nanostructure. This strategy provides a remarkably simple route to produce complex metallic nanostructures with controllable hollow interiors by means of the reaction of solid metal nanostructures, used as sacrificial templates (usually Ag [19, 64–68], but also Cu [69–71], Co [70, 72–77], Pd [78, 79], Mg [80] or alloys Pd-Cu [81]) and a precursor containing a relatively more noble metal ion (Au, Pd, or Pt), in a process by which the composition of the template is modified while retaining its initial morphology. Figure 2A shows the schematic illustration of the morphological and structural changes involved in the GRR between a Ag nanocube and $HAuCl_4$

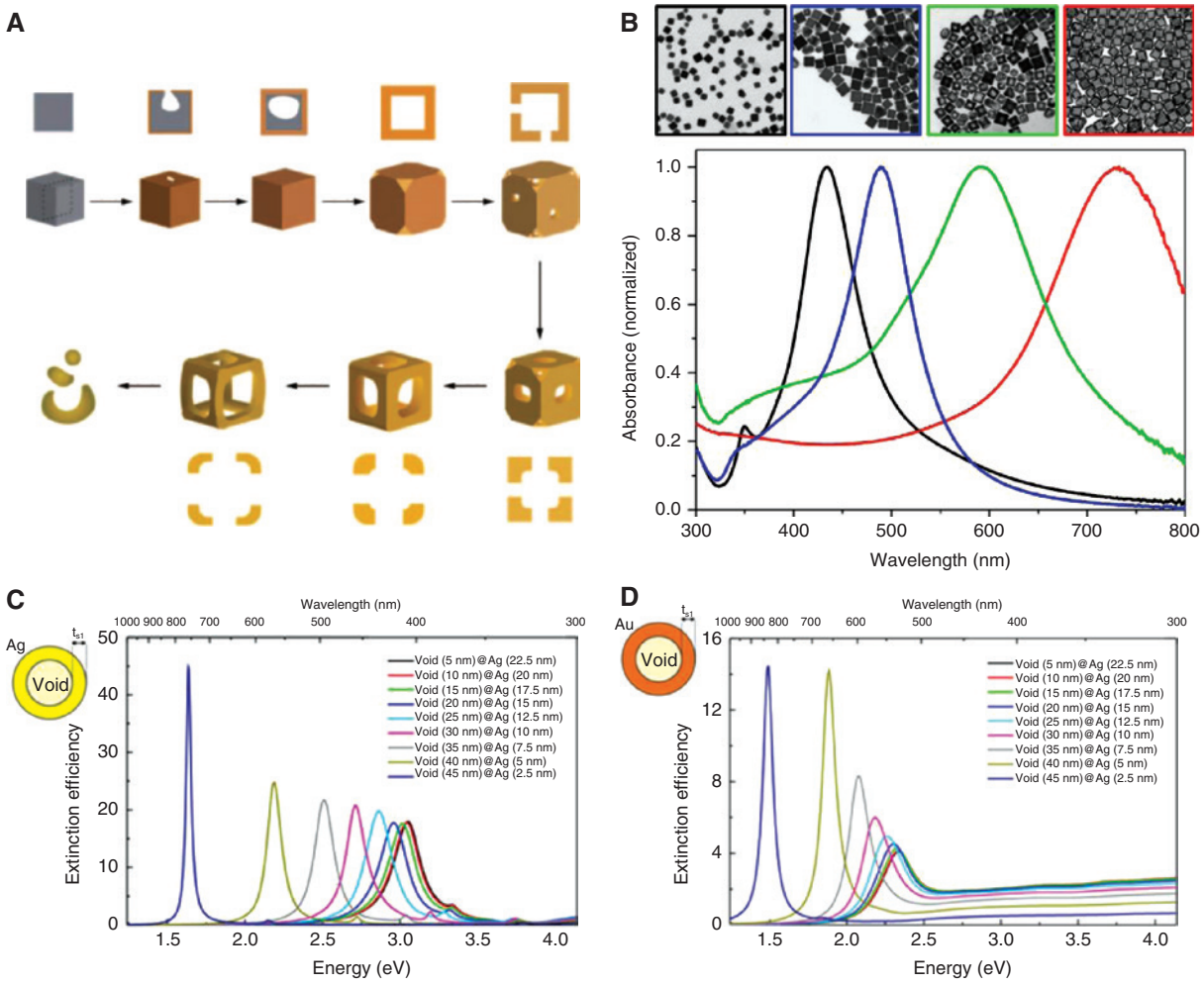

Figure 2: The mechanism of void formation during GRR reaction and its effects on optical properties. (A) Schematic illustration of the morphological and structural changes involved in the GRR between a silver nanocube and $HAuCl_4$. The cross-sectional views correspond to the plane along the dashed lines. The major steps of the reaction include the following: formation of a pinhole at one of the side faces; continuation of the GRR resulting in a partially hollow structure; enlargement of pores at the side faces; reduction of the ridge thickness; and finally fragmentation of the nanoframes (adapted with permission from Ref. [82], through the Creative Commons Attribution Noncommercial License). (B) UV-Vis spectra of Ag nanocubes (in black), core-shell Ag@A unanocubes (in blue), pinholed AuAg nanoboxes (in green) and single-walled AuAg nanoboxes (in red) along with their representative TEM images, revealing the shift of plasmon resonances with the formation of hollow nanostructures. (C) and (D) are the Mie scattering calculations revealing the effect of void size on the optical properties 50 nm Ag and Au nanospheres, respectively.

Brought to you by | Hospital Universitari Vall d'Hebron
Authenticated
Download Date | 3/7/19 12:30 PM

[82]. Recently, Goris et al. [83] showed the morphological transformations and elemental compositions of the nanostructures during the GRR of Ag by using 3D STEM-EDX tomography. Figure 2B shows the modification of plasmon resonances with increasing Au amount, thus, increasing the void size, where bulk UV-Vis spectra of solutions containing Ag nanocubes (in black), core-shell AgAu nanocubes (in blue), pinholed AuAg nanoboxes (in green), and single-walled AuAg nanoboxes (in red) are presented along with their representative transmission electron microscope (TEM) micrographs. As seen in this figure, the plasmon resonances shift to lower energies, i.e. higher wavelengths, as the void size increases, which is in accordance with the above-presented hybridization mechanism. Figure 2B already reveals the tunability of plasmon resonances by the changes in the void size. As a systematic approach of such modifications, we provide a series of Mie scattering calculations [84] on the 50 nm spherical Ag (Figure 2C) and Au (Figure 2D) nanoparticles with different void sizes and show the potential of tuning the plasmon resonances within a wide energy range from ultraviolet to near infrared regions.

Ag is the commonly used sacrificial template for the GRR due to a relatively low electrochemical potential and its well-established colloidal chemistry [70, 85]. In the GRR reaction with Ag, which rely on the different reduction potentials of two elemental metals, the atoms of the template NC oxidize and dissolve, while the ions of the more noble metal precursor are simultaneously reduced onto it. This reduction is initially confined to the vicinity of the template surface, leading to the nucleation, growth (and alloy) of the noble metal precursor, which forms a thin shell that oxidizes and dissolves the NC template, driving the formation of a pinhole that expands toward its center causing its dissolution. The first demonstration of GRR in the synthesis of hollow metal NCs was reported by Xia and co-workers in 2002 [86]. In this pioneering work, GRRs between Au^{3+} salt and pre-synthesized Ag NCs used as sacrificial templates led to the formation of hollow Au NCs with well-defined void spaces and crystalline walls. Although GRR is the most versatile method of preparing hollow metal NCs with controllable pore structures and compositions, the strategy has been also extended to the production of hollow semiconductor [87] and oxide NCs [88].

Since Xia's pioneering work, a wide variety of Au hollow NCs with controlled composition, morphology, and internal structure have been produced, with the only constraint of the favorable difference in the reduction potentials of the two metals involved in the reaction [17, 89]. The elemental composition of the final hollow NCs can be simply adjusted by selecting the nature of the sacrificial template, and the concentration, type, number, and order of addition of metal precursors involved in the reaction. Thus, in addition to AuAg hollow nanostructures, PtAg, PdAg [90], PdPt alloy nanocages [91, 92], and trimetallic PdAuAg hollow nanostructures with control of the spatial distributions of different metals [93] can also be prepared via the GRR by simply altering the order of addition for the salt precursors, which resulted in an improved tailoring of their optical and catalytic properties. Other hollow compositions such as PtAg bimetallic nanostructures [65] and PtAg@Pt core-shell single-crystal hollow NCs [67] have also been obtained via GRR between Ag templates and a Pt salt.

Beyond the final composition, the morphology of the hollow nanostructrures can easily be controlled by the choice of the template. As the deposition of precursor atoms takes place on the surface of the NC, the final hollow NC retains the shape and dimensions of the original template [86, 94], which allows the control of the morphology of the hollow structure [95]. Thus, Xia group has widely studied how Ag nanocubes synthesized by using a polyol process and then oxidized by an aqueous $HAuCl_4$ solution generate uniform Au nanoboxes or nanocages [64, 96–99]. Similarly, Ag nanowires have been widely exploited as templates for the preparation of hollow nanotubes via the GRR [86, 97, 100–104]. Other structures commonly obtained through the GRR between $HAuCl_4$ and the corresponding Ag template include nanorings [105, 106], nanoframes [107–109], and nanorattles [110–114]. A set of hollow AuAg nanostructures are shown in Figure 3.

Besides, the internal structure of the hollow nanostructures, in particular the porosity and thickness of the shell, can be easily tuned by controlling the de-alloying process in the later stages of the GRR. This control allows inducing morphological reconstructions, leading, for instance, to the formation of pinholes in the porous walls [97]. By coupling GRR with other chemical/physical processes complex hollow nanostructures, such as multi-walled NCs [102, 110], can be obtained. A recent review discusses advances on the use of GRR for generating complex hollow nanostructures with tunable and well-controlled properties [17].

Alternatively to GRR, hollow NCs with controlled voids interiors and shell thickness can be also obtained by the Kirkendall effect, which results from the difference of the solid-state diffusion rates of the reactants in an alloying or oxidation reaction. Although the first documented study by Ernest Kirkendall dates back 70 years ago [115], the (nanoscale) Kirkendall effect has recently become a powerful approach to the preparation of nanoscale

Brought to you by | Hospital Universitari Vall d'Hebron
Authenticated
Download Date | 3/7/19 12:30 PM

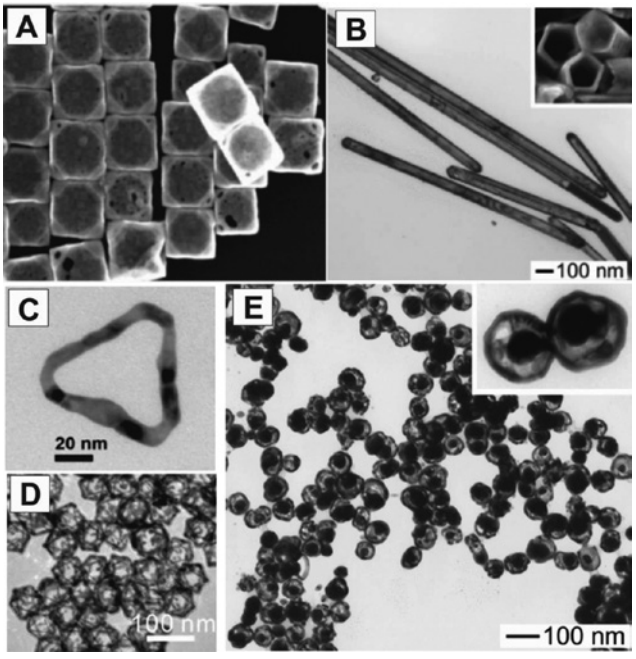

Figure 3: Electron microscopy images of various hollow nanostructures. (A) SEM image of AuAg nanoboxes. (B) TEM image of AuAg nanotubes (adapted with permission from Ref. [97], copyright 2004 American Chemical Society). (C) TEM image of an Au ring (reproduced with permission from Ref. [106], copyright 2014 Royal Society of Chemistry). (D) TEM image of AuAg octahedral nanoframes (reproduced with permission from Ref. [108], copyright 2012 American Chemical Society). (E) TEM image of nanorattles (reproduced with permission from Ref. [110], copyright 2004 American Chemical Society).

hollow structures. In this chemical transformation, metal NCs of controlled size, composition, and morphology are exposed to oxygen, phosphorus, sulfur, or selenium precursors under elevated temperatures resulting in a diffusion couple. As a result of the much faster outward diffusion of the metal cations than the inward diffusion of the anions, a flux of vacancies is created. When the vacancies supersaturate, they coalesce into a void which results in the production of hollow NCs with binary compositions. Since the first report in 2004 [116] on the synthesis of CoS and CoO hollow nanocrystals by sulfidation and oxidation of Co nanocrystals, several different kinds of hollow nanocrystals have been prepared by a similar approach that involves the nanoscale Kirkendall effect [117–121]. A recent review on the synthesis and characterization of hollow NCs through the nanoscale Kirkendall effect can be found in Ref. [117].

Although its use is limited for the production of noble metal hollow NCs, the simultaneous or sequential action of GRR and the Kirkendall effect has been found an interesting synthetic route for the production of polymetallic hollow nanocrystals with various morphologies and compositions. Thus, by using Ag NCs as templates, and Au, Pd, or Pt as oxidizing agents, Gonzalez et al. [19] showed the possibility to produce polymetallic multi-walled hollow NCs and other complex morphologies as shown in Figure 4. The method, based on the attacking and pitting of preformed NCs from the "inside out", is scalable and performed at room temperature, and results in very complex geometric interconnected multicavity hollow NCs.

3 Ultralocal plasmonic properties

Dark field microscopy is a commonly used technique for studying the plasmonic properties at a single nanoparticle level (providing that the nanoparticles are well dispersed on the substrate), however, it should be combined with a scanning electron microscope (SEM) or TEM to know the morphology of the studied nanoparticle and to ensure that the signal collected is generated from a single nanoparticle rather than agglomerates [122, 123]. Hu et al. conducted the first studies on the optical properties of individual hollow nanoparticles consisting of AuAg nanoboxes and nanocages by using Rayleigh scattering spectroscopy in a dark field microscope which was correlated with a SEM [124, 125]. Figure 5 shows the Rayleigh scattering spectra and SEM images of several AuAg nanocages as studied by Hu et al. [125] where {100} facets of the nanocages in Figure 5A,B and {111} facets of the nanocages in Figure 5C,D are in contact with the substrate. One can see the slight changes in the resonance energy and presence

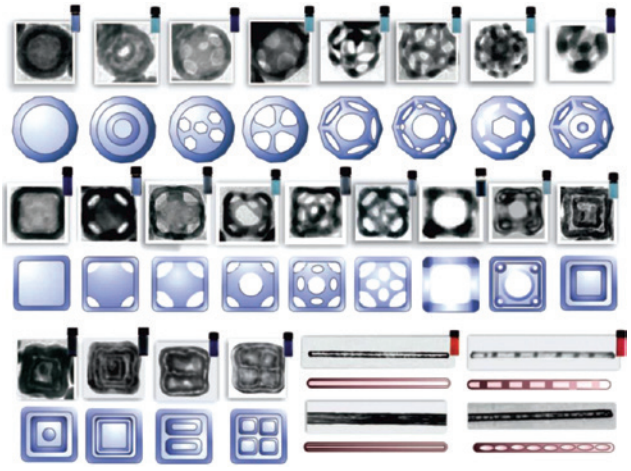

Figure 4: TEM images and schematic representation of the different morphologies produced by the simultaneous or sequential action of galvanic replacement reaction and the Kirkendall effect (adapted with permission from Ref. [19], copyright 2011 The American Association for the Advancement of Science).

Brought to you by | Hospital Universitari Vall d'Hebron
Authenticated
Download Date | 3/7/19 12:30 PM

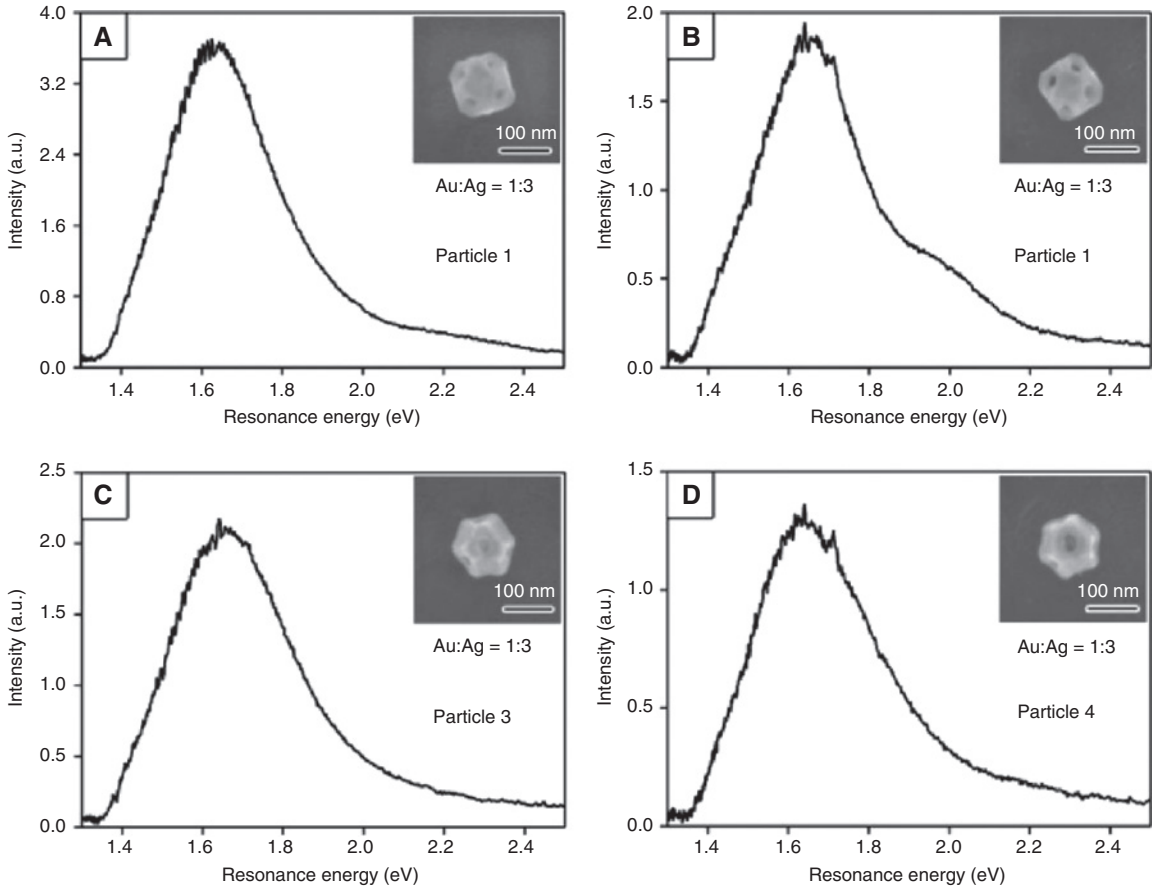

Figure 5: Correlated Rayleigh scattering spectra and SEM images of 4 different AuAg nanocages. AuAg nanocages in (A) and (B) are oriented as their [100] facets are in contact with the substrate, whereas [111] facets are in contact with the substrate for the AuAg nanocages in (C) and (D) (reproduced with permission from Ref. [125],copyright 2007 American Chemical Society).

of some additional shoulder peaks depending on the morphology of the AuAg nanocages [125]. Yang et al. [126] also studied the optical properties of individual hollow AuAg nanospheres and their dimers by using correlated optical single particle spectroscopy with TEM and revealed the nanostructures angle-dependent plasmon coupling.

As referred by the name of the technique, single nanoparticle spectroscopy studies can only provide information at the single nanoparticle level; however, it is also crucial to understand the distribution of different plasmon modes within the nanoparticles in order to fully elucidate its plasmonic properties. Cathodoluminescence spectroscopy in SEM or TEM and electron-energy loss spectroscopy in STEM are known to provide high spatial resolutions to study the local plasmonic properties of individual nanostructures [46]. In this review, we will focus on the latter technique.

A red shift in the plasmon resonances compared to the solid nanostructures is observed by UV-Vis spectroscopy while producing hollow nanostructures and this shift is related to the plasmon hybridization mechanism [17, 19, 89, 127, 128]. The first experimental demonstration of such hybridization/coupling at the nanoscale was performed by Kociak et al. [129] on anisotropic hollow nanoparticles of WS_2 by using EELS and later on the same group studied the plasmon coupling in some other nanotubes [130, 131]. It is worth noting that EELS has also been used recently for imaging plasmon hybridization in solid nanoparticle aggregates [132]. Experimental studies of the plasmonic properties of hollow metal nanostructures at the nanoscale by EELS proving the coupling of inner and outer modes, i.e. hybridization are conducted only during recent years [73, 133]. These results are discussed in more detail in the following paragraphs.

Utilization of EELS for characterization of plasmonic properties is well documented in the literature. In fact, EELS for plasmonics goes back to the first experimental studies leading to the discovery of plasmon resonance phenomena where most of the studies observed the energy losses of fast electrons passing through metal films [134–139]. The era of the application of EELS for plasmonics has changed since 2007, when Nelayah et al. [140] and Bosman et al. [141] reported, almost simultaneously,

Brought to you by | Hospital Universitari Vall d'Hebron
Authenticated
Download Date | 3/7/19 12:30 PM

first examples of spatial mapping the SPRs of individual nanoparticles at the nanometer scale by mono-chromated EELS in a STEM using the spectrum imaging (SI) technique developed by Jeanguillaume and Colliex in 1989 [142].

Ever since the above-mentioned precedent studies, EELS has been used to map plasmon resonances of different solid nanostructures including spherical nanoparticles, nanorods/nanowires, nanocubes, nanodisks, nanoprisms, nanostars, nanosquares, and nanodecahedra [31, 50, 143–162]. Along with its capability to give information with high spatial and energy resolutions, EELS has the ability to reveal full modal spectrum including dark plasmon modes, which are invisible to optical spectroscopy techniques, in coupled nanostructures [31, 145, 148, 152, 155, 163, 164]. Again all these studies were conducted on solid nanostructures and for more information on similar studies, the reader is referred to two recent comprehensive reviews by Kociak and Stephan [47] and Colliex et al. [165] on the application of EELS for plasmonics.

Although, EELS has been used intensively for the imaging of plasmon resonances in solid nanostructures, there are only a few studies dealing with the application of EELS for the plasmonic properties of hollow metal nanostructures [73, 133]. Prieto et al. [73] investigated the evolution of plasmon resonances in spherical hollow gold nanoparticles and gold nanorings by using EELS and related DDA simulations and have reported that as the aspect ratio between the wall thickness and diameter of the nanorings increases, plasmon resonances shift to lower energies in accordance with the plasmon hybridization mechanism and the scheme shown in Figure 1B [39].

Recently, we have reported the plasmonic properties of various cuboid hollow AuAg nanostructures synthesized via galvanic replacement [19] at the nanoscale by using EELS and BEM simulations and have provided experimental evidence of plasmon hybridization in such nanostructures. By reporting the ultralocal distribution of plasmon resonances, we have provided experimental insights about their enhanced plasmonic properties [133]. Figure 6 shows the structural and optical evolution of various cuboid nanostructures from solid Ag nanocubes to AuAg nanoframes, where it is clearly seen that plasmon resonances shift to lower energies with increasing void size. Generally, such an energy shift is the result of two main effects in such nanoparticles synthesized via GRR: (i) compositional effects due to AuAg alloying and (ii) morphological effects due to void formation. In order to better understand the extent of plasmon hybridization, i.e. voids, and to be able to distinguish them, if possible, from the compositional effects, we have simulated 50 nm Ag nanoboxes with various wall thicknesses (see Figure 6D). Our simulations revealed that the morphological changes are the dominant factor for the shift of plasmon resonance energies. As it is clearly seen in Figure 6D, plasmon resonances shift to lower energies with increasing void size even though there is no alloying, as suggested by the plasmon hybridization mechanism. The amount of the shift is higher for the thinner walls, where plasmon resonances barely shift for the 5 nm void but they shift about 0.8 eV as the void size increases from 40 to 45 nm due to strong hybridization [133].

Figure 7A shows the spectra and abundance maps of three plasmonic components of a single-walled AuAg nanobox (STEM image with red borders) which is 50 nm in size and has about 7 nm thick walls, confirming the postulation that the hollow nanostructures would generate homogeneously distributed plasmon resonances [127, 128]. These maps revealing the homogeneous spatial distribution of plasmon resonances in such a hollow nanostructure may be the explanation of their enhanced plasmonic properties for different applications such as sensing, as all the surface of the nanobox acts like a continuous "hot-spot" with intense plasmon excitations [133]. Spectra and abundance maps of three plasmonic components of an AuAg nanoframe (STEM image with green borders) which is 48 nm in size and has about 7 nm thick walls are shown in Figure 7B. These abundance maps, which are the first experimental representation for such metal nanostructures, showing the distribution of the plasmon resonances at the nanoscale clearly reveal the interaction of inner and outer plasmon fields in such hollow nanostructures. The experimental results are successfully correlated with BEM simulations (see Figure 7C for the nanoframe) both in 2D and in 3D with an assumption about the nanobox's/nanoframe's structural homogeneity [133].

In addition to the above-presented experimental results, several simulation studies by using DDA and FDTD have been conducted in order to understand the distribution of the plasmon resonances in individual or coupled hollow metal nanostructures [14, 127, 128, 166–171]. These simulation studies were usually used to explain the enhanced performance of the hollow nanostructures in applications like sensing and catalysis by revealing the distribution of plasmon resonances inside and around the nanostructures and calculating the generated electromagnetic fields [14, 127, 128]. For instance, Mahmoud and El-Sayed [127] experimentally studied the sensitivity of Au nanoframes with different lengths and wall thicknesses and concluded that the sensitivity factors increase as the aspect ratio, the ratio between the length and wall thickness, increases. Then, they have

Brought to you by | Hospital Universitari Vall d'Hebron
Authenticated
Download Date | 3/7/19 12:30 PM

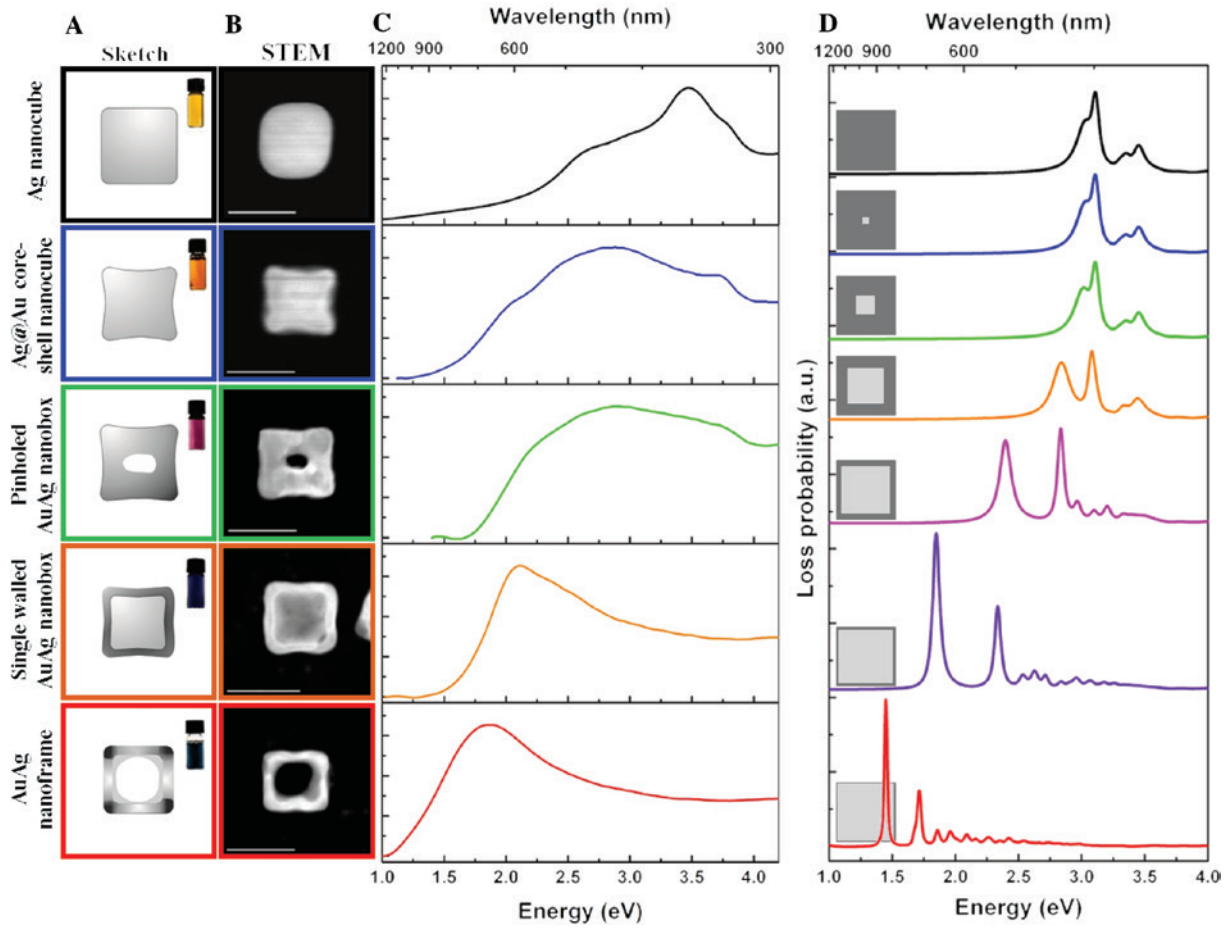

Figure 6: Structural and LSPR evolution of the AuAg nanostructures. (A) Structural sketches and corresponding solution colors from solid Ag nanocubes to single-walled AuAg nanobox and AuAg nanoframe. (B) HAADF STEM images of the nanostructures where SI EELS have been acquired (scale bars = 50 nm). (C) Zero-loss peak subtracted EEL spectra averaged over the areas of interests, i.e. EELS maps, showing the evolution of localized SPRs with structural changes. (D) BEM-simulated EEL spectra revealing the effect of void size for Ag nanostructures: 50 nm Ag nanocube (in black), 5 nm void (in blue), 15 nm void (in green), 30 nm void (in orange), 40 nm void (in magenta), 45 nm void (in purple), and 48 nm void (in red) (reproduced with permission from Ref. [133], copyright 2016 American Chemical Society).

used DDA simulations to correlate their experimental findings and found out that for nanoframes with similar aspect ratios, the magnitude of the red shift per unit change in wall thickness depends on the size of the nanoframe rather than being a constant value due to different intracavity surface coupling behavior [127].

As mentioned earlier, Ag nanostructures are known to have better plasmonic performance than those of Au [9, 14], as the plasmonic properties of Au nanostructures suffer a lot from the interband transitions as their onset partially overlaps with the LSPRs, causing a decrease in the intensity [10–12]. Mahmoud et al. [14] applied DDA simulations to calculate the plasmonic field intensity generated by individual Ag nanocubes and Au nanoframes or their dimers (as shown in Figure 8), revealing that Au nanoframes can generate plasmonic fields that are comparable to those of Ag nanocubes.

4 Applications of hollow nanostructures and advantages vs. solid counterparts

Hollow metal nanostructures have been used in many applications such as sensing, SERS, PTA of cancer, drug delivery, photoacoustic imaging, and catalysis over the years with performances better than their solid counter parts [14, 89, 127, 128, 133, 172–196]. Figure 9 shows the application of hollow metal nanostructures in various fields such as sensing (Figure 9A), catalysis (Figure 9B), SERS (Figure 9C), PTA of cancer (Figure 9D), drug delivery (Figure 9E), and photoacoustic imaging (Figure 9F). As seen in this figure, some of the applications are shown by experimental results (Figure 9A, C, and F) and some others are shown by representative sketches of the relevant mechanism (Figure 9B, D, and E).

Brought to you by | Hospital Universitari Vall d'Hebron
Authenticated
Download Date | 3/7/19 12:30 PM

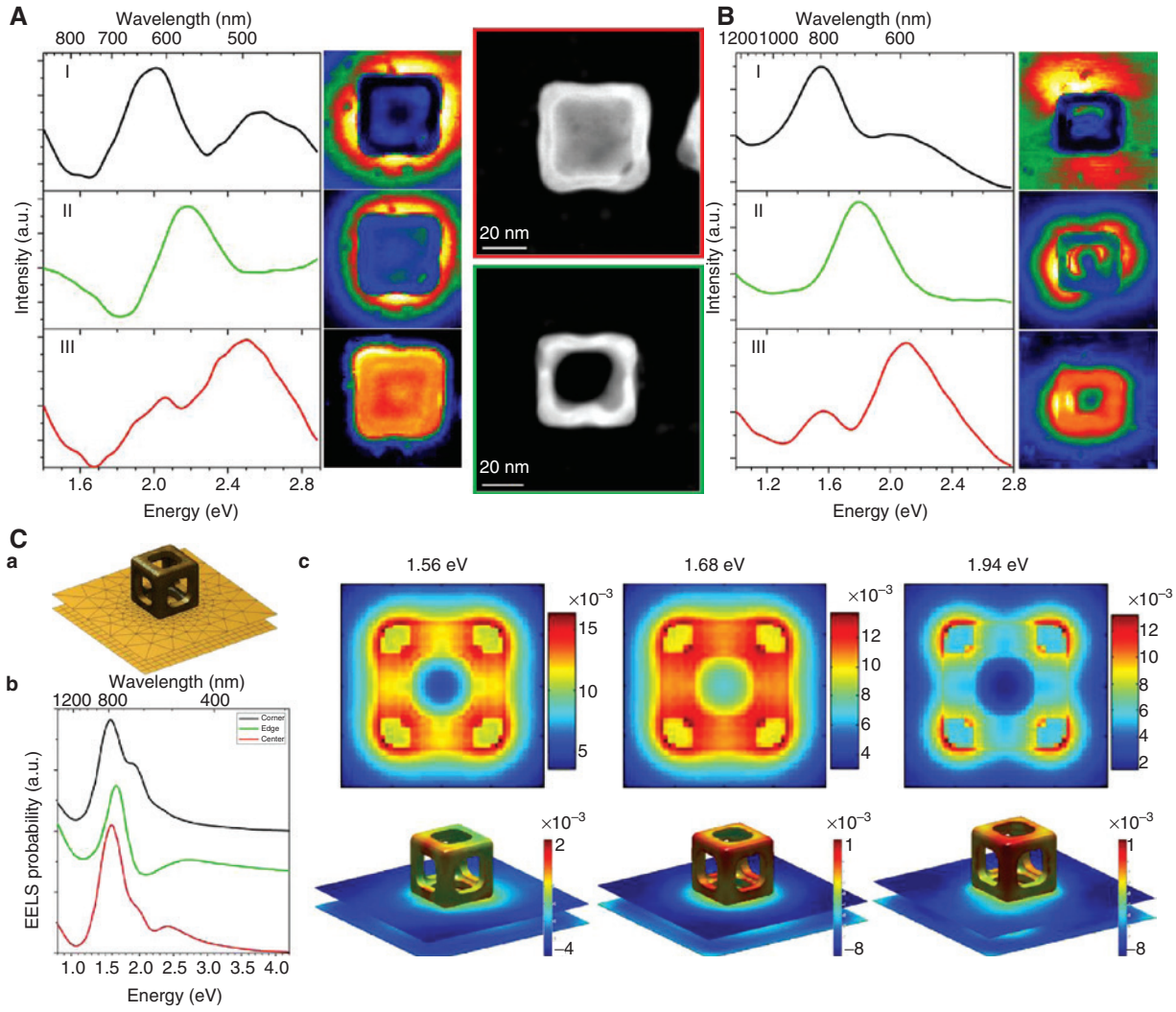

Figure 7: Plasmonic properties of single-walled AuAg nanobox and AuAg nanoframe. (A) Spectra and abundance maps of three plasmon components of the single-walled AuAg nanobox (marked with red), obtained by vertex component analysis (VCA) processing. (B) Spectra and abundance maps of three plasmon components of the AuAg nanoframe (marked with green), obtained by VCA processing. (C) BEM simulations of the AuAg nanoframe. (C-a) Structural model used during simulations. (C-b) Simulated local EEL spectra obtained from the corner, edge, and center of the nanoframe. (C-c) Simulated plasmon maps of three different LSPR modes located at 1.56, 1.68, and 1.94 eV along with their corresponding induced electric field intensity distribution with an edge beam excitation in 3D (lower row) (adapted with permission from Ref. [133], copyright 2016 American Chemical Society).

Label-free optical sensing with plasmonic nanoparticles is based on the detection of adsorbate-induced refractive index changes near or on the nanoparticles, which change the dielectric constant of the surrounding medium and can be measured by using UV-visible extinction spectroscopy [2, 3, 197]. Adsorbate-induced shifts in LSPR can be expressed as $\Delta\lambda_{max}$, which simply equals to [198]:

$$\Delta\lambda_{max} = \lambda_{max} < \text{after} > - \lambda_{max} < \text{before} > .$$

The sensitivity of plasmonic nanoparticles can be quantified by using the term sensitivity factor (SF), which is defined as the nanometers of shift in the LSPR peak of the nanoparticle per the refractive index unit (nm/RIU) of the surrounding medium [2]. Thus, a higher SF depicts the generalization of larger shifts in the LSPR peak of the nanoparticle with smaller changes in the refractive index of the surrounding analytes.

As already stated, hollow nanostructures are known to be more effective in label-free sensing compared to their solid counterparts [14, 133, 190, 199]. Sun and Xia [199] compared the sensitivity of solid Au nanospheres and Au nanoshells and reported almost a seven-fold increase in the SF while using the Au nanoshells. By calculating the amount of 1-HDT molecules covering the

Brought to you by | Hospital Universitari Vall d'Hebron
Authenticated
Download Date | 3/7/19 12:30 PM

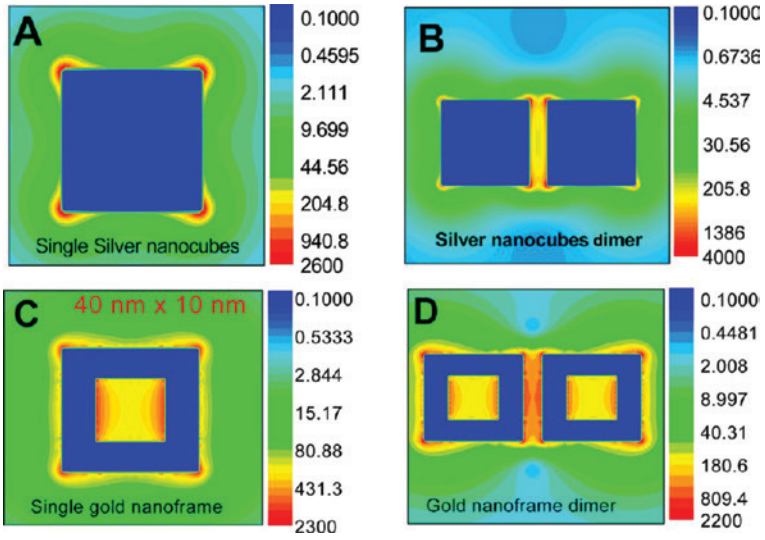

Figure 8: DDA calculated plasmonic field distributions of solid Ag nanocubes and gold nanoframes. (A) individual Ag nanocube, (B) dimer of Ag nanocubes, (C) single Au nanoframe, and (D) dimer of Au nanoframes (reproduced from Ref. [14], copyright 2014 American Chemical Society).

Au nanoshells, they have estimated a detection limit of about 27 nM by using conventional absorption spectrometers [199]. Mahmoud et al. [14] tabulated a five-fold increased SF when comparing Au nanocubes and hollow Au nanocages. Recently, we have reported a ~4-fold increase in the sensitivities of single-walled nanoboxes compared to solid Au nanoparticles against conjugation events with bovine serum albumin (BSA) protein and its antibodies thanks to the enhancement of the localized electromagnetic field around the hollow nanoboxes that allows easy and direct detection of binding events on their vicinity [133]. Satija et al. [190] prepared hollow gold nanospheres based fiber-optic sensors having a 1.5-fold enhancement in sensitivity compared to solid Au nanoparticle-based sensors. They have been also used as immunosensors and reported a maximum of four-fold better detection limit compared to other Au-based biosensors [190].

Surface enhanced Raman spectroscopy, a technique where the localization and amplification of incident light fields by SPRs lead to an enhanced Raman scattering, is arguably one of the most common applications of plasmonic nanostructures since its discovery about 40 years ago [200–202]. Thanks to the developments in the spectroscopic information techniques, nanofabrication routines and novel detection schemes, SERS has been established as a powerful tool in sensing and detecting at molecular level [3, 203]. Since the pioneering works of Nie and Emory [204] and Kneipp et al. [205] reporting the single molecule detection via SERS, it has been extensively exploited for the detection of different molecules and disease markers at the molecular level [206–212].

Hollow Au or AuAg nanostructures provide enhanced SERS activity compared to that of solid Ag nanoparticles [178, 179, 187, 188, 191, 213, 214]. Schwartzberg et al. [188] compared the SERS activity of 30 nm hollow Au nanoparticles with those of solid Ag nanoparticles and reported a 10-fold increase in the SERS signal consistency and by using these hollow gold nanostructures as pH sensors, they have shown about two-fold increase in resolution and 10-fold increase in precision over the Ag nanoparticle-based SERS probes. Guo et al. [191] applied hollow gold chip based SERS probes for detection of melamine in milk in order to monitor the adulteration of milk by melamine. Hollow gold chip generates much more (about four-fold) intense Raman signal compared to the solid chip revealing its effectiveness even at the low (nM level) concentrations where there is no SERS signal for the case of solid nanoparticles [191]. Yi et al. [179] studied the synthesis of AuAg bimetallic hollow nanospheres and their application in SERS and reported that the hollow nanospheres generate intense Raman signals than those of solid Au seed nanoparticles, SiO_2@Au core@shell nanoshells, SiO_2@AuAg bimetallic nanoshells during the detection of 1.0×10^{-8} M R6G. Olson et al. [187] synthesized hollow AuAg double-shell nanospheres for SERS and observed that bimetallic hollow AuAg nanospheres produced about four-fold intense SERS signal over hollow Au nanospheres, suggesting the effect of Ag. However, Ag shell did not yield the same enhancement for the solid Au nanospheres revealing that the enhancement in the SERS signal was a

Brought to you by | Hospital Universitari Vall d'Hebron
Authenticated
Download Date | 3/7/19 12:30 PM

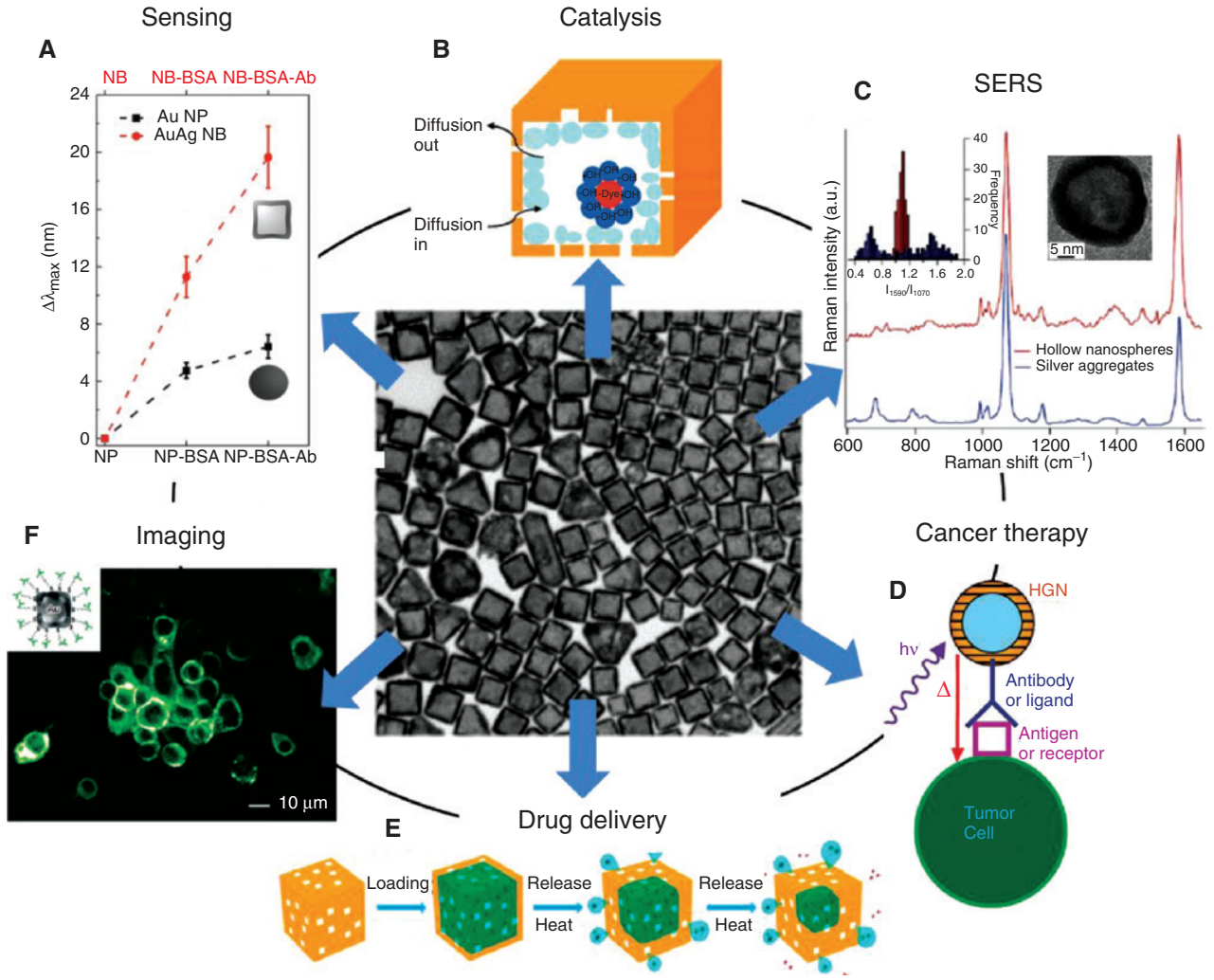

Figure 9: Various applications of hollow nanostructures. (A) Comparison of sensitivities of solid Au nanoparticles and single-walled AuAg nanoboxes against the conjugation events with BSA protein and its antibodies (adapted with permission from Ref. [133], copyright 2016 American Chemical Society). (B) Photodegredation reaction inside the Au nanocage with pores allowing the diffusion (reproduced with permission from Ref. [184], copyright 2009 American Chemical Society). (C) Single-particle SERS spectra of 4-mercaptobenzoic acid on hollow Au nanospheres and Ag aggregates (reproduced with permission from Ref. [188], copyright 2006 American Chemical Society). (D) Schematic illustration of the photothermal ablation cancer therapy mechanism: hollow Au nanostructures (HGN) are linked to the target cancer cells through antibody-antigen or ligand-receptor interactions and the heat (Δ) generated by light illumination is used for thermal imaging and/or destruction of the cancer cell (reproduced with permission from Ref. [176], copyright 2010 American Chemical Society). (E) Schematic illustration of the loading of Au nanocage with 1-tetradecanol dye/drug and its release triggered by light illumination (reproduced with permission from Ref. [183], copyright 2013 American Chemical Society). (F) A fluorescence image of human breast carcinoma epithelial cells (SK-BR-3) obtained after surface treatment with the anti-HER2 antibodies and incubation with fluorescence-labeled IgG, where insets show the schematic of antibody conjugation to the Au nanocages (reproduced with permission from Ref. [185], copyright 2005 American Chemical Society).

combination of compositional effects by Ag addition and generation of intense plasmon fields in hollow nanostructures due to plasmon hybridization [187].

Plasmonic nanoparticles have the ability to absorb light and convert it to heat by a mechanism called photothermal effect [175]. When the plasmonic nanostructures, i.e. Au nanocages, excited by a near-infrared region (NIR) illumination, they generate plasmon resonances which decay into hot electrons with energies between vacuum level and Fermi level. The heat generation due to the surface hot electrons is then released to the media causing an increase in the temperature [215, 216]. Thanks to the photothermal effect, plasmonic nanoparticles have been used intensively in different nanomedicine applications such as imaging, drug delivery, cancer diagnosis, and photo-ablation therapy [89, 172, 173, 175–178, 182, 183, 185, 186, 192, 193, 195, 217–225].

Brought to you by | Hospital Universitari Vall d'Hebron
Authenticated
Download Date | 3/7/19 12:30 PM

As mentioned earlier, plasmonic nanostructures used in nanomedicine applications are Au-based due to their bioinertness and easiness of modification of their surfaces with different materials such as antibodies and peptides for different applications [89]. Most of these Au-based nanostructures are nanorods and hollow nanostructures as their plasmon resonances can be finely tuned in the NIR, where the blood and soft tissue are relatively transparent [222]. Moreover, the hollow nanostructures can be used as suitcases for drug delivery applications [175, 217, 220, 222]. You et al. [222] reported bifunctional use of ~40 nm hollow Au nanospheres (HAuNS) for photothermal ablation of cancer cells and drug release upon NIR light irradiation, revealing their excellent drug delivery properties. They have reported that HAuNS can be loaded about four times more DOX compared to the solid AuNPs, which can also be easily released upon NIR laser irradiation, along with the much higher photothermal heat generation capabilities compared to their solid counterparts [222]. Owing to their strong and tunable absorption in the NIR and high stability, hollow Au nanocages are used as optical imaging contrast agents [182, 185], enabling efficient optical detection of disease markers [193, 223].

One of the most important exploitation of plasmonic heat generation by photothermal effect is their application for the PTA of cancer [176]. As mentioned earlier, the blood and soft tissue are relatively transparent in the NIR and nanostructures to be used in PTA should have strong, narrow, and tunable NIR absorption along with other features such as small size and spherical or near-spherical shapes [176]. Small size and near-spherical shapes are crucial for the efficient intracellular uptake, as cell penetration of nanostructures such as Au nanorods, although they have strong NIR absorption, are known to be less effective compared to spherical nanoparticles [226]. Hollow Au nanostructures simultaneously fulfill all the relevant requisites for an efficient PTA. Melancon et al. [224] were the first to use hollow Au nanostructures (~30 nm in size) in PTA, where they have reported efficient destruction of A431 tumor cells treated with anti-epidermal growth factor receptor (EGFR)-HAuNs with near-infrared laser irradiation. As a control experiment, they have studied the cell viability of cells treated with anti-EGFR-HAuNS alone (no laser), laser alone, or laser-irradiated IgG-HAuNS and did not observe any indication of destruction of tumor cells [224]. Similarly, Lu et al. [225] showed the application of targeted ~40 nm HAuNS as efficient *in vivo* PTA of melanoma. Au et al. [186] conducted a quantitative study for the application of ~65 nm Au nanocages in PTA of breast cancer cells by NIR laser irradiation and reported about 35% cellular damage within 5 min under optimized condition such as the laser power and cell harvest duration. As evident from all these studies, HAuNS holds a great promise in the therapy of different kinds of cancers as a less harmful alternative to standard chemotherapy [227].

Another field of application where hollow nanostructures perform better than their solid counterparts is catalysis [14, 93, 111, 184, 194, 228–232]. It should be noted here that the Pt- or Pd-based nanostructures have better catalytic activity or the addition of these elements to the AuAg nanostructures increase their catalytic activity, yet they have poor plasmonic properties [14, 93, 111, 194, 224, 226]. In the following, we focus on the application of plasmonic, Au-based hollow catalysts. Zeng et al. [231] compared the catalytic activity of different Au-based nanostructures including nanocages, nanoboxes, and solid nanoparticles and reported that Au-based nanocages are catalytically more active than both the nanoboxes and nanoparticles. Such high activitiy of Au nanocages can be related to the fact that these nanostructures have ultrathin walls, high content of Au and provide accessibility of both inner and outer surfaces through the pores in the walls [231]. Khalavka et al. [111] reported an improved plasmon sensitivity and catalytic activity of rod-shaped nanorattles compared to Au nanorods, where plasmon resonances of the nanorattles show greater sensitivity to changes in the dielectric environment, and they show higher catalytic activity. Wu et al. [232] studied the catalytic activity of different AgAu bimetallic hollow nanoshells and solid nanoparticles and reported that the hollow nanostructures exhibit higher catalytic activity than the solid nanoparticles even though solid nanoparticles have higher Au content, indicating the dominant effect of the morphology for the catalysis. El-Sayed and co-workers [184, 194, 224, 226] reported that enhanced catalytic activity of the hollow nanostructures can be attributed to the so-called nanocage effect, where the catalytic reaction takes place inside the nanocage. Figure 9B shows the schematic representation of a photocatalytic reaction that takes place inside the nanocage [184]. Certain conditions should be provided in order to obtain optimum reaction rates in such nanocages: (i) Ag should have high surface area on the inner wall of the nanocage to generate sufficient hydroxyl radicals after its oxidation to Ag_2O; (ii) the pore sizes should be large enough to allow the diffusion of the reactants in and out of the nanocage but in the meantime should be small enough to keep the high steady state concentrations of the radicals; (iii) the pores inside the cage should be in the size regime which provides optimum collision rate between the reactants [184].

Brought to you by | Hospital Universitari Vall d'Hebron
Authenticated
Download Date | 3/7/19 12:30 PM

5 Summary and outlook

In the present review we have shown how metallic nanostructures have a great ability to generate SPRs. In particular, hollow nanostructures have been presented as promising plasmonic materials with enhanced properties vs. their solid counterparts, thanks to the plasmon hybridization mechanism. The hybridization of the plasmons results in the enhancement of the plasmon fields along with more homogeneous distribution as well as the reduction of LSPR quenching due to absorption. We have shown how GRR is one of the most effective methods to obtain the synthesis of hollow metal nanostructures. We have reviewed the advancements on the characterization of plasmonic properties in hollow nanostructures, covering the single nanoparticle experiments, nanoscale characterization via EELS and modeling and simulation studies. Finally, we have shown several examples of the applications, i.e. sensing, SERS, PTA of cancer, drug delivery, or catalysis where hollow nanostructures perform better than their solid counterparts.

Although there has been remarkable progress on the synthesis, characterization, and applicability of plasmonic hollow nanostructures during the recent years, there still remain several challenges to be solved in order to exploit such nanoparticles in industrial applications. The advantage of hollow plasmonic nanostructures mainly comes from the presence of two surfaces (internal and external) and hybridization among them, along with the presence of cavities and pores at the walls. Thanks to the progress in the synthetic routes, we can now master the issues like wall thickness and void size, yet perfect control on the size and distribution of the surface pores, which are as important as the void size while determining the final plasmonic properties, is a crucial challenge to overcome in the future. Again, we have the means to precisely tune the plasmonic properties of hollow nanostructures over a wide range. Such ability comes as an output of having full control over the synthesis of template materials, GRR conditions, and surface functionalities of both the template and hollow nanostructures. So far, these rather complex routines are conducted at the laboratory scale with impressive controls over each step. It should be pointed out that achieved precise controls for the synthesis of gram scale nanostructures are mainly thanks to the usage of high purity reagents. The next step forward would be to optimize these conditions in the mass scales along with using cheaper reagents in order to meet with the requirements for industrial applications. Moreover, we postulate that as our understanding on the local plasmonic properties of hollow nanostructures gets deeper, it paves the way to the design and synthesis of application specific hollow nanostructures with highly enhanced properties. Therefore, we need more systematic studies on the nanoscale plasmonic properties of hollow nanostructures, which then can be used as feedbacks for the synthesis as well as the applications.

Acknowledgments: J.A. and A.G. acknowledge the funding from Generalitat de Catalunya 2014 SGR 1638 and Spanish MICINN project e-ATOM (MAT2014-51480-ERC). J.P., N.G.B., and V.P. acknowledge financial support from the Generalitat de Catalunya 2014-SGR-612, Spanish MICINN (MAT2012-33330) and European Community (EU-FP7) through the FutureNanoNeeds project. N.G.B. acknowledges financial support by MINECO through the Ramon y Cajal program (RYC-2012- 10991) and by the European Commission Seventh Framework Programme (FP7) through the Marie Curie Career Integration Grant (322153-MINE). ICN2 acknowledges support from the Severo Ochoa Program (MINECO, Grant SEV-2013-0295).

References

[1] Schuller J, Barnard ES, Cai W, Jun YC, White JS, Brongersma ML. Plasmonics for extreme light concentration and manipulation. Nature Mater 2010;9:193–204.
[2] Mayer KM, Hafner JH. Localized surface plasmon resonance sensors. Chem Rev 2011;111:3828–57.
[3] Haes AJ, Haynes CL, McFarland AD, Schatz GC, Van Duyne RP, Zou S. Plasmonic materials for surface-enhanced sensing and spectroscopy. MRS Bull 2005;30:368–75.
[4] Atwater HA, Polman A. Plasmonics for improved photovoltaic devices. Nature Mater 2010;9:205–13.
[5] Fang N, Lee H, Zhang X. Sub-diffraction-limited optical imaging with a silver superlens. Science 2005;308:534–7.
[6] Sorger VJ, Zhang X. Spotlight on plasmon lasers. Science 2011;333:709–10.
[7] Shalaev VM. Optical negative-index metamaterials. Nature Photon 2007;1:41–8.
[8] Chang DE, Sorensen AS, Hemmer PR, Lukin MD. Quantum optics with surface plasmons. Phys Rev Lett 2006;97:053002.
[9] Rycenga M, Cobley CM, Zeng J, Li W, Moran CH, Zhang Q, Qin D, Xia Y. Controlling the synthesis and assembly of silver nanostructures for plasmonic applications. Chem Rev 2011;111:3669–712.
[10] Perner M, Bost P, Lemmer U, von Plessen G, Feldmann J, Becker U, Mennig M, Schmitt M, Schmidt H. Optically induced damping of the surface plasmon resonance in gold colloids. Phys Rev Lett 1997;78:2192–5.
[11] Amendola V, Bakr MO, Stellacci F. A study of the surface plasmon resonance of silver nanoparticles by the discrete dipole approximation method: effect of shape, size, structure, and assembly. Plasmonics 2010;5:85–97.
[12] Noguez C. Surface plasmons on metal nanoparticles: the inuence of shape and physical environment. J Phys Chem C 2007;111:3806–19.

Brought to you by | Hospital Universitari Vall d'Hebron
Authenticated
Download Date | 3/7/19 12:30 PM

[13] Prodan E, Radloff C, Halas NJ, Nordlander P. A hybridization model for the plasmon response of complex nanostructures. Science 2003;302:419–22.
[14] Mahmoud MA, O'Neil D, El-Sayed MA. Hollow and solid metal nanostructures in sensing and in nanocatalysis. Chem Mater 2014;26:44–58.
[15] Bastús NG, Gonzalez E, Esteve J, Piella J, Patarroyo J, Merkoçi F, Puntes V. Exploring new synthetic strategies for the production of advanced complex inorganic nanocrystals. Z Physik Chem 2015;229:65–83.
[16] Wang X, Feng J, Bai Y, Zhang Q, Yin Y. Synthesis, properties, and applications of hollow micro-/nanostructures. Chem Rev Article ASAP (2016), DOI: 10.1021/acs.chemrev.5b00731.
[17] Xia X, Wang Y, Ruditskiy A, Xia Y. 25th anniversary article: galvanic replacement: a simple and versatile route to hollow nanostructures with tunable and well-controlled properties. Adv Mater 2013;25:6313–33.
[18] Cobley CM, Xia Y. Engineering the properties of metal nanostructures via galvanic replacement reactions. Mater Sci Eng R 2010;70:44–62.
[19] Gonzalez E, Arbiol J, Puntes VF. Carving at the nanoscale: sequential galvanic exchange and kirkendall growth at room temperature. Science 2011;334:1377–80.
[20] Prodan E, Nordlander P. Plasmon hybridization in spherical nanoparticles. J Chem Phys 2004;120:5444–54.
[21] Nordlander P, Oubre C, Prodan E, Li K, Stockman MI. Plasmon hybridization in nanoparticle dimers. Nano Lett 2004;4: 899–903.
[22] Zhang S, Bao K, Halas NJ, Xu H, Nordlander P. Substrate-induced fano resonances of a plasmonic nanocube: a route to increased-sensitivity localized surface plasmon resonance sensors revealed. Nano Lett 2011;11:1657–63.
[23] Halas NJ, Lal S, Chang WS, Link S, Nordlander P. Plasmons in strongly coupled metallic nanostructures. Chem Rev 2011;111:3913–61.
[24] Jain PK, Huang W, El-Sayed MA. On the universal scaling behavior of the distance decay of plasmon coupling in metal nanoparticle pairs: a plasmon ruler equation. Nano Lett 2007;7:2080–8.
[25] Ghosh SK, Pal T. Interparticle coupling effect on the surface plasmon resonance of gold nanoparticles: from theory to applications. Chem Rev 2007;107:4797–862.
[26] Jain PK, El-Sayed MA. Surface plasmon coupling and its universal size scaling in metal nanostructures of complex geometry: elongated particle pairs and nanosphere trimers. J Phys Chem C 2008;112:4954–60.
[27] Garcia De Abajo FJ. Nonlocal effects in the plasmons of strongly interacting nanoparticles, dimers, and waveguides. J Phys Chem C 2008;112:17983–7.
[28] Jain PK, El-Sayed MA. Plasmonic coupling in noble metal nanostructures. Chem Phys Lett 2010;487:153–64.
[29] Shao L, Woo KC, Chen H, Jin Z, Wang J, Lin HQ. Angle- and energy-resolved plasmon couplings in gold nanorod dimers. ACS Nano 2010;4:3053–62.
[30] Grillet N, Manchon D, Bertorelle F, Bonnet C, Broyer M, Cottancin E, Lermé J, Hillenkamp M, Pellarin M. Plasmon coupling in silver nanocube dimers: resonance splitting induced by edge rounding. ACS Nano 2011;5:9450–62.
[31] Koh AL, Bao K, Khan I, Smith WE, Kothleitner G, Nordlander P, Maier SA, McComb DW. Electron energy-loss spectroscopy (EELS) of surface plasmons in single silver nanoparticles and dimers: influence of beam damage and mapping of dark modes. ACS Nano 2009;3:3015–22.
[32] Nordlander P, Prodan E. Plasmon hybridization in nanoparticles near metallic surfaces. Nano Lett 2004;4:2209–13.
[33] Yang SC, Kobori H, He CL, Lin MH, Chen HY, Li C, Kanehara M, Teranishi T, Gwo S. Plasmon hybridization in individual gold nanocrystal dimers: direct observation of bright and dark modes. Nano Lett 2010;10:632–7.
[34] Slaughter LS, Wu Y, Willingham BA, Nordlander P, Link S. Effects of symmetry breaking and conductive contact on the plasmon coupling in gold nanorod dimers. ACS Nano 2010;4:4657–66.
[35] Osberg KD, Harris N, Ozel T, Ku JC, Schatz GC, Mirkin CA. Systematic study of antibonding modes in gold nanorod dimers and trimers. Nano Lett 2014;14:6949–54.
[36] Prodan E, Nordlander P. Structural tunability of the plasmon resonances in metallic nanoshells. Nano Lett 2003;3:543–7.
[37] Brandl DW, Oubre C, Nordlander P. Plasmon hybridization in nanoshell dimers. J Chem Phys 2005;123:24701.
[38] Jain PK, El-Sayed MA. Universal scaling of plasmon coupling in metal nanostructures: extension from particle pairs to nanoshells. Nano Lett 2007;7:2854–8.
[39] Halas N. Playing with plasmons: tuning the optical resonant properties of metallic nanoshells. MRS Bull 2005;30:362–7.
[40] Prodan E, Nordlander P, Halas NJ. Electronic structure and optical properties of gold nanoshells. Nano Lett 2003;3:1411–15.
[41] Oubre C, Nordlander P. Optical properties of metallodielectric nanostructures calculated using the finite difference time domain method. J Phys Chem B 2004;108:17740–7.
[42] Kulkarni V, Prodan E, Nordlander P. Quantum plasmonics: optical properties of a nanomatryushka. Nano Lett 2013;13: 5873–9.
[43] Xia Y, Halas NJ. Shape-controlled synthesis and surface plasmonic properties of metallic nanoparticles. MRS Bull 2005;30:338–44.
[44] Liz-Marzán LM. Tailoring surface plasmons through the morphology and assembly of metal nanoparticles. Langmuir 2006;22:32–41.
[45] Zhang J, Zhang L. Nanostructures for surface plasmons. Adv Opt Phot 2012;4:157–321.
[46] García de Abajo FJ. Optical excitations in electron microscopy. Rev Mod Phys 2010;82:209–75.
[47] Kociak M, Stephan O. Mapping plasmons at the nanometer scale in an electron microscope, Chem Soc Rev 2014;43:3865–83.
[48] Draine BT, Flatau PJ. Discrete-dipole approximation for scattering calculations. J Opt Soc Am A 1994;11:1491–9.
[49] Geuquet N, Henrard L. EELS and optical response of a noble metal nanoparticle in the frame of a discrete dipole approximation. Ultramicroscopy 2010;110:1075–80.
[50] Guiton BS, Iberi V, Li S, Leonard DN, Parish CM, Kotula PG, Varela M, Schatz GC, Pennycook SJ, Camden JP. Correlated optical measurements and plasmon mapping of silver nanorods. Nano Lett 2011;11:3482–8.
[51] García de Abajo FJ, Howie A. Relativistic electron energy loss and electron-induced photon emission in inhomogeneous dielectrics. Phys Rev Lett 1998;80:5180–3.
[52] García de Abajo FJ, Howie A. Retarded field calculation of electron energy loss in inhomogeneous dielectrics. Phys Rev B 2002;65:1–17.

Brought to you by | Hospital Universitari Vall d'Hebron
Authenticated
Download Date | 3/7/19 12:30 PM

[53] Hohenester U. Simulating electron energy loss spectroscopy with the MNPBEM toolbox. Comput Phys Commun 2014;185:1177–87.
[54] Caruso F, Caruso RA, Möhwald H. Nanoengineering of inorganic and hybrid hollow spheres by colloidal templating. Science 1998;282:1111–14.
[55] Zhong Z, Yin Y, Gates B, Xia Y. Preparation of mesoscale hollow spheres of TiO_2 and SnO_2 by templating against crystalline arrays of polystyrene beads. Adv Mater 2000;12:206–9.
[56] Choi WS, Koo HY, Kim DY. Facile fabrication of core-in-shell particles by the slow removal of the core and its use in the encapsulation of metal nanoparticles. Langmuir 2008;24:4633–6.
[57] Liu J, Qiao SZ, Liu H, Chen J, Orpe A, Zhao D, Lu GQ. Extension of The Stöber Method to the preparation of monodisperse resorcinol–formaldehyde resin polymer and carbon spheres. Angew Chem Int Ed 2011;50:5947–51.
[58] Tu W, Zhou Y, Liu Q, Tian Z, Gao J, Chen X, Zhang H, Liu J, Zou Z. Robust hollow spheres consisting of alternating titania nanosheets and graphene nanosheets with high photocatalytic activity for CO_2 conversion into renewable fuels. Adv Funct Mater 2012;22:1215–21.
[59] Kim SW, Kim M, Lee WY, Hyeon T. Fabrication of hollow palladium spheres and their successful application to the recyclable heterogeneous catalyst for Suzuki coupling reactions. J Am Chem Soc 2002;124:7642–3.
[60] Yu XY, Yu L, Shen L, Song X, Chen H, Lou XW. General formation of MS (M = Ni, Cu, Mn) box-in-box hollow structures with enhanced pseudocapacitive properties. Adv Funct Mater 2014;24:7440–6.
[61] Titirici MM, Antonietti M, Thomas A. A generalized synthesis of metal oxide hollow spheres using a hydrothermal approach. Chem Mater 2006;18:3808–12.
[62] Sasidharan M, Nakashima K. Core–shell–corona polymeric micelles as a versatile template for synthesis of inorganic hollow nanospheres. Acc Chem Res 2014;47:157–67.
[63] Huang C, Jiang J, Lu M, Sun L, Meletis EI, Hao Y. Capturing electrochemically evolved nanobubbles by electroless deposition. A facile route to the synthesis of hollow nanoparticles. Nano Lett 2009;9:4297–301.
[64] Skrabalak SE, Au L, Li X, Xia Y. Facile synthesis of Ag nanocubes and Au nanocages. Nat Protocols 2007;2:2182–90.
[65] Zhang W, Yang J, Lu X. Tailoring galvanic replacement reaction for the preparation of Pt/Ag bimetallic hollow nanostructures with controlled number of voids. ACS Nano 2012;6:7397–405.
[66] Sieb NR, Wu NC, Majidi E, Kukreja R, Branda NR, Gates BD. Hollow metal nanorods with tunable dimensions, porosity, and photonic properties. ACS Nano 2009;3:1365–72.
[67] Gonzalez E, Merkoci F, Arenal R, Arbiol J, Esteve J, Bastús NG, Puntes V. Enhanced reactivity of high-index surface platinum hollow nanocrystals. J Mater Chem A 2016;4:200–8.
[68] Polavarapu L, Liz-Marzan LM. Growth and galvanic replacement of silver nanocubes in organic media. Nanoscale 2013;5:4355–61.
[69] Liu S, Zheng X, Song L, Liu W, Yao T, Sun Z, Lin Y, Wei S. Partial-surface-passivation strategy for transition-metal-based copper-gold nanocage. Chem Commun 2016;52:6617–20.
[70] Gilroy KD, Farzinpour P, Sundar A, Hughes RA, Neretina S. Sacrificial templates for galvanic replacement reactions: design criteria for the synthesis of pure Pt nanoshells with a smooth surface morphology. Chem Mater 2014;26:3340–47.
[71] Mohl M, Dobo D, Kukovecz A, Konya Z, Kordas K, Wei JQ, Vajtai R, Ajayan PM. Formation of CuPd and CuPt bimetallic nanotubes by galvanic replacement reaction. J Phys Chem C 2011;115:9403–9.
[72] Nafria R, Genç A, Ibáñez M, Arbiol J, de la Piscina PR, Homs N, Cabot A. Co–Cu nanoparticles: synthesis by galvanic replacement and phase rearrangement during catalytic activation. Langmuir 2016;32:2267–76.
[73] Prieto M, Arenal R, Henrard L, Gomez L, Sebastian V, Arruebo M. Morphological tunability of the plasmonic response: from hollow gold nanoparticles to gold nanorings. J Phys Chem C 2014;118:28804–11.
[74] Schwartzberg AM, Olson TY, Talley CE, Zhang JZ. Synthesis, characterization, and tunable optical properties of hollow gold nanospheres. J Phys Chem B 2006;110:19935–44.
[75] Schwartzberg AM, Olson TY, Talley CE, Zhang JZ. Gold nanotubes synthesized via magnetic alignment of cobalt nanoparticles as templates. J Phys Chem C 2007;111:16080–2.
[76] Preciado-Flores S, Wang D, Wheeler DA, Newhouse R, Hensel JK, Schwartzberg A, Wang L, Zhu J, Barboza-Flores M, Zhang JZ. Highly reproducible synthesis of hollow gold nanospheres with near infrared surface plasmon absorption using PVP as stabilizing agent. J Mater Chem 2011;21:2344–50.
[77] Adams S, Thai D, Mascona X, Schwartzberg AM, Zhang JZ. Key factors affecting the reproducibility of synthesis and growth mechanism of near-infrared absorbing hollow gold nanospheres. Chem Mater 2014;26:6805–10.
[78] Liu M, Zheng Y, Xie S, Li N, Lu N, Wang J, Kim MJ, Guo L, Xia Y. Facile synthesis of Pd-Ir bimetallic octapods and nanocages through galvanic replacement and co-reduction, and their use for hydrazine decomposition. Phys Chem Chem Phys 2013;15:11822–9.
[79] Xie S, Jin M, Tao J, Wang Y, Xie Z, Zhu Y, Xia Y. Synthesis and characterization of Pd@MxCu1–x (M=Au, Pd, and Pt) nanocages with porous walls and a yolk–shell structure through galvanic replacement reactions. Chem Eur J 2012;18:14974–80.
[80] Li X, Liu H, Yang J, Qiao SZ, Du XW. Pure gold nanocages by galvanic replacement reaction of magnesium nanoparticles. RSC Adv 2014;4:1185–8.
[81] Yao Y, He DS, Lin Y, Feng X, Wang X, Yin P, Hong X, Zhou G, Wu Y, Li Y. Modulating fcc and hcp ruthenium on the surface of palladium–copper alloy through tunable lattice mismatch. Angew Chem Int Ed 2016;128:5591–5.
[82] Au L, Chen Y, Zhou F, Camargo PH, Lim B, Li ZY, Ginger DS, Xia Y. Synthesis and optical properties of cubic gold nanoframes. Nano Res 2008;1:441–9.
[83] Goris B, Polavarapu L, Bals S, van Tendeloo G, Liz-Marzán LM. Monitoring galvanic replacement through three-dimensional morphological and chemical mapping. Nano Lett 2014;14:3220–6.
[84] Juluri BK, Huang J, Jensen L. Extinction, scattering and absorption efficiencies of single and multilayer nanoparticles (2010). https://nanohub.org/resources/8228. Accessed September 2015.
[85] Bastús NG, Merkoçi F, Piella J, Puntes V. Synthesis of highly monodisperse citrate-stabilized silver nanoparticles of up to 200 nm: kinetic control and catalytic properties. Chem Mater 2014;26:2836–46.
[86] Sun Y, Mayers BT, Xia Y. Template-engaged replacement reaction: a one-step approach to the large-scale synthesis of metal nanostructures with hollow interiors. Nano Lett 2002;2:481–5.

Brought to you by | Hospital Universitari Vall d'Hebron
Authenticated
Download Date | 3/7/19 12:30 PM

[87] Xiao F, Yoo B, Lee KH, Myung NV. Synthesis of Bi_2Te_3 nanotubes by galvanic displacement. J Am Chem Soc 2007;129:10068–9.
[88] Oh MH, Yu T, Yu SH, Lim B, Ko KT, Willinger MG, Seo DH, Kim BH, Cho MG, Park JH, Kang K, Sung YE, Pinna N, Hyeon T. Galvanic replacement reactions in metal oxide nanocrystals. Science 2013;340:964–8.
[89] Skrabalak SE, Chen J, Sun Y, Lu X, Au L, Cobley CM, Xia Y. Gold nanocages: synthesis, properties, and applications. Acc Chem Res 2008;41:1587–95.
[90] Chen J, Wiley B, McLellan J, Xiong Y, Li ZY, Xia Y. Optical properties of Pd–Ag and Pt–Ag nanoboxes synthesized via galvanic replacement reactions. Nano Lett 2005;5:2058–62.
[91] Zhang H, Jin M, Liu H, Wang J, Kim MJ, Yang D, Xie Z, Liu J, Xia Y. Facile synthesis of Pd–Pt alloy nanocages and their enhanced performance for preferential oxidation of CO in excess hydrogen. ACS Nano 2011;5:8212–22.
[92] Hong JW, Kang SW, Choi BS, Kim D, Lee SB, Han SW. Controlled synthesis of Pd–Pt alloy hollow nanostructures with enhanced catalytic activities for oxygen reduction. ACS Nano 2012;6:2410–9.
[93] Cobley CM, Campbell DJ, Xia Y. Tailoring the optical and catalytic properties of gold-silver nanoboxes and nanocages by introducing palladium. Adv Mater 2008;20:748–52.
[94] Polavarapu L, Mourdikoudis S, Pastoriza-Santos I, Pérez-Juste J. Nanocrystal engineering of noble metals and metal chalcogenides: controlling the morphology, composition and crystallinity. Cryst Eng Commun 2015;17:3727–62.
[95] Xia Y, Xiong Y, Lim B, Skrabalak SE. Shape-controlled synthesis of metal nanocrystals: simple chemistry meets complex physics? Angew Chem Int Ed 2009;48:60–103.
[96] Sun Y, Xia Y. Shape-controlled synthesis of gold and silver nanoparticles. Science 2002;298:2176–9.
[97] Sun Y, Xia Y. Mechanistic study on the replacement reaction between silver nanostructures and chloroauric acid in aqueous medium. J Am Chem Soc 2004;126:3892–901.
[98] Chen J, McLellan JM, Siekkinen A, Xiong Y, Li ZY, Xia Y. Facile synthesis of gold–silver nanocages with controllable pores on the surface. J Am Chem Soc 2006;128:14776–7.
[99] Lu X, Au L, McLellan J, Li ZY, Marquez M, Xia Y. Fabrication of cubic nanocages and nanoframes by dealloying Au/Ag Alloy nanoboxes with an aqueous etchant based on $Fe(NO_3)_3$ or NH_4OH. Nano Lett 2007;7:1764–9.
[100] Sun Y. Silver nanowires – unique templates for functional nanostructures. Nanoscale 2010;2:1626–42.
[101] Sun Y, Mayers B, Xia Y. Metal nanostructures with hollow interiors. Adv Mater 2003;15:641–6.
[102] Sun Y, Xia Y. Multiple-walled nanotubes made of metals. Adv Mater 2004;16:264–8.
[103] Sun Y, Wang Y. Monitoring of galvanic replacement reaction between silver nanowires and $HAuCl_4$ by in situ transmission X-ray microscopy. Nano Lett 2011;11:4386–92.
[104] Ye S, Marston G, McLaughlan JR, Sigle DO, Ingram N, Freear S, Baumberg JJ, Bushby RJ, Markham AF, Critchley K, Coletta PL, Evans SD. Engineering gold nanotubes with controlled length and near-infrared absorption for theranostic applications. Adv Funct Mater 2015;25:2117–27.
[105] Sun Y, Xia Y. Triangular nanoplates of silver: synthesis, characterization, and use as sacrificial templates for generating triangular nanorings of gold. Adv Mater 2003;15:695–9.
[106] Ghosh T, Satpati B, Senapati D. Characterization of bimetallic core-shell nanorings synthesized via ascorbic acid-controlled galvanic displacement followed by epitaxial growth. J Mater Chem C 2014;2:2439–47.
[107] Métraux GS, Cao YC, Jin R, Mirkin CA. Triangular nanoframes made of gold and silver. Nano Lett 2003;3:519–22.
[108] Hong X, Wang D, Cai S, Rong H, Li Y. Single-crystalline octahedral Au–Ag nanoframes. J Am Chem Soc 2012;134:18165–8.
[109] McEachran M, Keogh D, Pietrobon B, Cathcart N, Gourevich I, Coombs N, Kitaev V. Ultrathin gold nanoframes through surfactant-free templating of faceted pentagonal silver nanoparticles. J Am Chem Soc 2011;133:8066–9.
[110] Sun Y, Wiley B, Li ZY, Xia Y. Synthesis and optical properties of nanorattles and multiple-walled nanoshells/nanotubes made of metal alloys. J Am Chem Soc 2004;126:9399–406.
[111] Khalavka Y, Becker J, Sonnichsen C. Synthesis of rod-shaped gold nanorattles with improved plasmon sensitivity and catalytic activity. J Am Chem Soc 2009;131:1871–5.
[112] Tsai MF, Chang SHG, Cheng FY, Shanmugam V, Cheng YS, Su CH, Yeh CS. Au nanorod design as light-absorber in the first and second biological near-infrared windows for in vivo photothermal therapy. ACS Nano 2013;7:5330–42.
[113] Chen Z, Yu D, Huang Y, Zhang Z, Liu T, Zhan J. Tunable SERS-tags-hidden gold nanorattles for theranosis of cancer cells with single laser beam. Sci Rep 2014;4:6709.
[114] Mahmoud MA. Optical properties of gold nanorattles: evidences for free movement of the inside solid nanosphere. J Phys Chem C 2014;118:10321–8.
[115] Kirkendall EO. Diffusion of zinc in alpha brass. Trans Am Inst Min Metall Eng 1942;147:104–9.
[116] Yin Y, Rioux RM, Erdonmez CK, Hughes S, Somorjai GA, Alivisatos AP. Formation of hollow nanocrystals through the nanoscale Kirkendall effect. Science 2004;304:711–14.
[117] Wang W, Dahl M, Yin Y. Hollow nanocrystals through the nanoscale Kirkendall effect. Chem Mater 2013;25:1179–89.
[118] Tang Y, Ouyang M. Tailoring properties and functionalities of metal nanoparticles through crystallinity engineering. Nature Mater 2007;6:754–9.
[119] Wang W, Goebl J, He L, Aloni S, Hu Y, Zhen L, Yin Y. Epitaxial growth of shape-controlled Bi_2Te_3–Te heterogeneous nanostructures. J Am Chem Soc 2010;132:17316–24.
[120] Cabot A, Puntes VF, Shevchenko E, Yin Y, Balcells L, Marcus MA, Hughes SM, Alivisatos AP. Vacancy coalescence during oxidation of iron nanoparticles. J Am Chem Soc 2007;129:10358–60.
[121] Chiang RK, Chiang RT. Formation of hollow Ni_2P nanoparticles based on the nanoscale Kirkendall effect. Inorg Chem 2007;46:369–71.
[122] Hu M, Novo C, Funston A, Wang H, Staleva H, Zou S, Mulvaney P, Xia Y, Hartland GV. Dark-field microscopy studies of single metal nanoparticles: understanding the factors that influence the linewidth of the localized surface plasmon resonance. J Mater Chem 2008;18:1949–60.
[123] Rodríguez-Fernández I, Novo C, Myroshnychenko V, Funston AM, Sánchez-Iglesias A, Pastoriza-Santos I, Pérez-Juste J, de Abajo FJG, Liz-Marzán LM, Mulvaney P. Spectroscopy, imaging, and modeling of individual gold decahedra. J Phys Chem C 2009;113:18623–31.
[124] Hu M, Petrova H, Sekkinen AR, Chen J, McLellan JM, Li ZY, Marquez M, Li X, Xia Y, Hartland GV. Optical properties of

Brought to you by | Hospital Universitari Vall d'Hebron
Authenticated
Download Date | 3/7/19 12:30 PM

Au-Ag nanoboxes studied by single nanoparticle spectroscopy. J Phys Chem B 2006;110:19923–8.
[125] Hu M, Chen J, Marquez M, Xia Y, Hartland GV. Correlated Rayleigh scattering spectroscopy and scanning electron microscopy studies of Au-Ag bimetallic nanoboxes and nanocages. J Phys Chem C 2007;111:12558–65.
[126] Yang L, Yan B, Reinhard BM. Correlated optical spectroscopy and transmission electron microscopy of individual hollow nanoparticles and their dimers. J Phys Chem C 2008;112:15989–96.
[127] Mahmoud MA, El-Sayed MA. Gold nanoframes: very high surface plasmon fields and excellent near-infrared sensors. J Am Chem Soc 2010;132:12704–10.
[128] Mahmoud MA, Snyder B, El-Sayed MA. Surface plasmon fields and coupling in the hollow gold nanoparticles and surface-enhanced Raman spectroscopy. Theory and experiment. J Phys Chem C 2010;114:7436–43.
[129] Kociak M, Stephan O, Henrard L, Charbois V, Rothschild A, Tenne R, Colliex C. Experimental evidence of surface-plasmon coupling in anisotropic hollow nanoparticles. Phys Rev Lett 2001;87:075501.
[130] Stephan O, Taverna D, Kociak M, Suenaga K, Henrard L, Colliex C. Dielectric response of isolated carbon nanotubes investigated by spatially resolved electron energy-loss spectroscopy: from multiwalled to single-walled nanotubes. Phys Rev B 2002;66:155422.
[131] Taverna D, Kociak M, Charbois V, Henrard L. Electron energy-loss spectrum of an electron passing near a locally anisotropic nanotube. Phys Rev B 2002;66:235419.
[132] Quillon SC, Cherqui C, Montoni NP, Li G, Camden JP, Masiello DJ. Imaging plasmon hybridization in metal nanoparticle aggregates with electron energy-loss spectroscopy. J Phys Chem C Article ASAP (2016), DOI: 10.1021/acs.jpcc.6b02170.
[133] Genç A, Patarroyo J, Sancho-Parramon J, Arenal R, Duchamp M, Gonzalez EE, Henrard L, Bastús NG, Dunin-Borkowski RE, Puntes VF, Arbiol J. Tuning the plasmonic response up: hollow cuboid metal nanostructures. ACS Photonics 2016;3:770–9.
[134] Pines D, Bohm D. A collective description of electron interactions: II. Collective vs individual particle aspects of the interactions. Phys Rev 1952;85:338–53.
[135] Ritchie RH. Plasma losses of fast electrons in thin films. Phys Rev 1957;106:874–81.
[136] Powell CJ, Swan JB. Origin of the characteristic electron energy losses in aluminum. Phys Rev 1959;115:869–75.
[137] Powell CJ, Swan JB. Origin of the characteristic electron energy losses in magnesium. Phys Rev 1959;116:81–3.
[138] Powell CJ, Swan JB. Effect of oxidation on the characteristic loss spectra of aluminium and magnesium. Phys Rev 1960;118:640–3.
[139] Stern EA, Ferrell RA. Surface plasma oscillations of a degenerate electron gas. Phys Rev 1960;120:130–6.
[140] Nelayah J, Kociak M, Stephan O, de Abajo FJG, Tencé M, Henrard L, Taverna D, Pastoriza-Santos I, Liz-Marzán LM, Colliex C. Mapping surface plasmons on a single metallic nanoparticle. Nature Phys 2007;3:348–53.
[141] Bosman M, Keast VJ, Watanabe M, Maaroof AI, Cortie MB. Mapping surface plasmons at the nanometre scale with an electron beam. Nanotechnology 2007;18:165505.
[142] Jeanguillaume C, Colliex C. Spectrum-image: the next step in EELS digital acquisition and processing. Ultramicroscopy 1989;28:252–7.
[143] Scholl JA, Koh AL, Dionne JA. Quantum plasmon resonances of individual metallic nanoparticles. Nature 2012;483:421–7.
[144] Barrow SJ, Rossouw D, Funston AM, Botton GA, Mulvaney P. Mapping bright and dark modes in gold nanoparticle chains using electron energy loss spectroscopy. Nano Lett 2014;14:3799–808.
[145] Chu MW, Myroshnychenko V, Chen CH, Deng JP, Mou CY, Garcia de Abajo FJ. Probing bright and dark surface-plasmon modes in individual and coupled noble metal nanoparticles using an electron beam. Nano Lett 2009;9:399–404.
[146] Nicoletti O, Wubs M, Mortensen NA, Sigle W, van Aken PA, Midgley PA. Surface plasmon modes of a single silver nanorod: an electron energy loss study. Opt Express 2011;19:15371–9.
[147] Rossouw D, Couillard M, Vickery J, Kumacheva E, Botton GA. Multipolar plasmonic resonances in silver nanowire antennas imaged with a subnanometer electron probe. Nano Lett 2011;11:1499–504.
[148] Bigelow NW, Vaschillo A, Iberi V, Camden JP, Masiello DJ. Characterization of the electron- and photon-driven plasmonic excitations of metal nanorods. ACS Nano 2012;6:7497–504.
[149] Mazzucco S, Geuquet N, Jian Y, Stéphan O, Van Roy W, Van Dorpe P, Henrard L, Kociak M. Ultralocal modification of surface plasmons properties in silver nanocubes. Nano Lett 2012;12:1288–94.
[150] Goris B, Guzzinati G, Fernandez-Lopez C, Pérez-Juste J, Liz-Marzán LM, Trügler A, Hohenester U, Verbeeck J, Bals S, Van Tendeloo G. Plasmon mapping in Au@Ag nanocube assemblies. J Phys Chem C 2014;118:15356–62.
[151] Nicoletti O, de la Pena F, Leary RK, Holland DJ, Ducati C, Midgley PA. Three-dimensional imaging of localized surface plasmon resonances of metal nanoparticles. Nature 2013;502:80–4.
[152] Schmidt FP, Ditlbacher H, Hohenester U, Hohenau A, Hofer F, Krenn JR. Dark plasmonic breathing modes in silver nanodisks. Nano Lett 2012;12:5780–3.
[153] Schmidt FP, Ditlbacher H, Hofer F, Krenn JR, Hohenester U. Morphing a plasmonic nanodisk into a nanotriangle. Nano Lett 2014;14:4810–15.
[154] Schaffer B, Grogger W, Kothleitner G, Hofer F. Comparison of EFTEM and STEM EELS plasmon imaging of gold nanoparticles in a monochromated TEM. Ultramicroscopy 2010;110:1087–93.
[155] Duan H, Fernandez A, Bosman M, Maier SA, Yang JKW. Nanoplasmonics: classical down to the nanometer scale. Nano Lett 2012;12:1683–9.
[156] Ringe E, DeSantis CJ, Collins SM, Duchamp M, Dunin-Borkowski RE, Skrabalak SE, Midgley PA. Resonances of nanoparticles with poor plasmonic metal tips. Sci Rep 2015;5:17431.
[157] Morla-Folch J, Guerrini L, Pazos-Perez N, Arenal R, Alvarez-Puebla RA. Synthesis and optical properties of homogeneous nanoshurikens. ACS Photonics 2014;1:1237–44.
[158] Mazzucco S, Stephan O, Colliex C, Pastoriza-Santos I, Liz-Marzan LM, Garcia de Abajo J, Kociak M. Spatially resolved measurements of plasmonic eigenstates in complex-shaped, asymmetric nanoparticles: gold nanostars. Eur Phys J Appl Phys 2011;54:33512.

Brought to you by | Hospital Universitari Vall d'Hebron
Authenticated
Download Date | 3/7/19 12:30 PM

[159] Myroshnychenko V, Nelayah J, Adamo G, Geuquet N, Rodríguez-Fernández J, Pastoriza-Santos I, MacDonald KF, Henrard L, Liz-Marzán LM, Zheludev NI, Kociak M, García de Abaj FJ. Plasmon spectroscopy and imaging of individual gold nanodecahedra: a combined optical microscopy, cathodoluminescence, and electron energy-loss spectroscopy study. Nano Lett 2012;12:4172–80.
[160] Collins SM, Ringe E, Duchamp M, Saghi Z, Dunin-Borkowski RE, Midgley PA. Eigenmode tomography of surface charge oscillations of plasmonic nanoparticles by electron energy loss spectroscopy. ACS Photonics 2015;2:1628–35.
[161] Bellido EP, Manjavacas A, Zhang Y, Cao Y, Nordlander P, Botton GA. Electron energy-loss spectroscopy of multipolar edge and cavity modes in silver nanosquares. ACS Photonics 2016;3:428–33.
[162] Arenal R, Henrard L, Roiban L, Ersen O, Burgin J, Treguer-Delapierre M. Local plasmonic studies on individual core–shell gold–silver and pure gold nano-bipyramids. J Phys Chem C 2014;118:25643–50.
[163] Koh AL, Fernandez-Dominguez AI, McComb DW, Maier SA, Yang JKW. High-resolution mapping of electron-beam-excited plasmon modes in lithographically defined gold nanostructures. Nano Lett 2011;11:1323–30.
[164] Haberfehlner G, Trugler A, Schmidt FP, Hörl A, Hofer F, Hohenester U, Kothleitner G. Correlated 3D nanoscale mapping and simulation of coupled plasmonic nanoparticles. Nano Lett 2015;15:7726–30.
[165] Colliex C, Kociak M, Stephan O. Electron energy loss spectroscopy imaging of surface plasmons at the nanometer scale. Ultramicroscopy 2016;162:A1–24.
[166] Hao E, Li S, Bailey RC, Zou S, Schatz GC, Hupp JT. Optical properties of metal nanoshells. J Phys Chem B 2004;108:1224–29.
[167] Qian J, Liu C, Wang W, Chen J, Li Y, Xu J, Sun Q. Effect of edge rounding on the extinction properties of hollow metal nanoparticles. Plasmonics 2013;8:955–62.
[168] Chandra M, Dowgiallo AM, Knappenberger KL. Controlled plasmon resonance properties of hollow gold nanosphere aggregates. J Am Chem Soc 2010;132:15782–9.
[169] Zhang ZS, Yang ZJ, Liu XL, Li M, Zhou L. Multiple plasmon resonances of Au/Ag alloyed hollow nanoshells. Scr Mater 2010;63:1193–6.
[170] De Angelis F, Malerba M, Patrini M, Miele E, Das G, Toma A, Zaccaria RP, Di Fabrizio E. 3D hollow nanostructures as building blocks for multifunctional plasmonics. Nano Lett 2013;13:3553–8.
[171] Xu X, Yi Z, Li X, Wang Y, Geng X, Luo J, Luo B, Yi Y, Tang Y. Discrete dipole approximation simulation of the surface plasmon resonance of core/shell nanostructure and the study of resonance cavity effect. J Phys Chem C 2012;116:24046–53.
[172] Dykman L, Khlebtov N. Gold nanoparticles in biomedical applications: recent advances and perspectives. Chem Soc Rev 2012;41:2256–82.
[173] Chen J, Yang M, Zhang Q, Cho EC, Cobley CM, Kim C, Glaus C, Wang LV, Welch MJ, Xia Y. Gold nanocages: a novel class of multifunctional nanomaterials for theranostic applications. Adv Funct Mater 2010;20:3684–94.
[174] Cao M, Wang M, Gu N. Optimized surface plasmon resonance sensitivity of gold nanoboxes for sensing applications. J Phys Chem C 2009;113:1217–21.
[175] Xia Y, Li W, Cobley CM, Chen J, Xia X, Zhang Q, Yang M, Cho EC, Brown PK. Gold nanocages: from synthesis to theranostic applications. Acc Chem Res 2011;44:914–24.
[176] Zhang JZ. Biomedical applications of shape-controlled plasmonic nanostructures: a case study of hollow gold nanospheres for photothermal ablation therapy of cancer. J Phys Chem Lett 2010;1:686–95.
[177] Cobley CM, Chen J, Cho EC, Wang LV, Xia Y. Gold nanostructures: a class of multifunctional materials for biomedical applications. Chem Soc Rev 2011;40:44–56.
[178] Adams S, Zhang JZ. Unique optical properties and applications of hollow gold nanospheres (HGNs). Coord Chem Rev 2016;320–321:18–37.
[179] Yi Z, Xu X, Li X, Luo J, Wu W, Tang Y, Yi Y. Facile preparation of Au/Ag bimetallic hollow nanospheres and its application in surface-enhanced Raman scattering. Appl Surf Sci 2011;258:212–17.
[180] Mahmoud MA. Surface-enhanced Raman spectroscopy of double-shell hollow nanoparticles: electromagnetic and chemical enhancements. Langmuir 2013;29:6253–61.
[181] Liu XW, Lin J, Jiang TF, Zhu ZF, Zhan QQ, Qian J, He S. Surface plasmon properties of hollow AuAg alloyed triangular nanoboxes and its applications in SERS imaging and potential drug delivery. Prog Electromagn Res 2012;128:35–53.
[182] Li W, Brown PK, Wang LV, Xia Y. Gold nanocages as contrast agents for photoacoustic imaging. Contrast Media Mol Imaging 2011;6:370–7.
[183] Tian L, Gandra N, Singamaneni S. Monitoring controlled release of payload from gold nanocages using surface enhanced Raman scattering. ACS Nano 2013;7:4252–60.
[184] Yen CW, Mahmoud MA, El-Sayed MA. Photocatalysis in gold nanocage nanoreactors. J Phys Chem A 2009;113:4340–5.
[185] Chen J, Saeki F, Wiley BJ, Cang H, Cobb MJ, Li ZY, Au L, Zhang H, Kimmey MB, Li X, Xia Y. Gold nanocages: bioconjugation and their potential use as optical imaging contrast agents. Nano Lett 2005;5:473–7.
[186] Au L, Zheng D, Zhou F, Li ZY, Li X, Xia Y. A quantitative study on the photothermal effect of immuno gold nanocages targeted to breast cancer cells. ACS Nano 2008;2:1645–52.
[187] Olson TY, Scwartzberg AM, Orme CA, Talley CE, O'Connel B, Zhang JZ. Hollow gold-silver double-shell nanospheres: structure, optical absorption, and surface-enhanced Raman scattering. J Phys Chem C 2008;112:6319–29.
[188] Schwartzberg AM, Oshlro TY, Zhang JZ, Huser T, Talley CE. Improving nanoprobes using surface-enhanced raman scattering from 30-nm hollow gold particles. Anal Chem 2006;78:4732–6.
[189] Chon H, Lee S, Son SW, Oh CH, Choo J. Highly sensitive immunoassay of lung cancer marker carcinoembryonic antigen using surface-enhanced raman scattering of hollow gold nanospheres. Anal Chem 2009;81:3029–34.
[190] Satija J, Tharion J, Mukherji S. Facile synthesis of size and wavelength tunable hollow gold nanostructures for the development of a LSPR based label-free fiber-optic biosensor. RSC Adv 2015;5:69970–9.
[191] Guo Z, Cheng Z, Li R, Chen L, Lv H, Zhao B, Choo J. One-step detection of melamine in milk by hollow gold chip based on surface-enhanced Raman scattering. Talanta 2014;122:80–4.

Brought to you by | Hospital Universitari Vall d'Hebron
Authenticated
Download Date | 3/7/19 12:30 PM

[192] You J, Zhang P, Hu F, Du Y, Yuan H, Zhu J, Wang Z, Zhou J, Li C. Near-infrared light-sensitive liposomes for the enhanced photothermal tumor treatment by the combination with chemotherapy. Pharm Res 2014;31:554–65.
[193] Skrabalak SE, Au L, Lu X, Li X, Xia Y. Gold nanocages for cancer detection and treatment. Nanomedicine 2007;2:657–8.
[194] Mahmoud MA, El-Sayed MA. Time dependence and signs of the shift of the surface plasmon resonance frequency in nanocages elucidate the nanocatalysis mechanism in hollow nanoparticles. Nano Lett 2011;11:946–53.
[195] Melancon MP, Zhou M, Li C. Cancer theranostics with near-infrared light-activatable multimodal nanoparticles. Acc Chem Res 2011;44:947–56.
[196] Jain PK, Huang X, El-Sayed IH, El-Sayed MA. Noble metals on the nanoscale: optical and photothermal properties and some applications in imaging, sensing, biology, and medicine. Acc Chem Res 2008;41:1578–86.
[197] Anker JN, Hall WP, Lyandres O, Shah NC, Zhao J, Van Duyne RP. Biosensing with plasmonic nanosensors, Nature Mater 2008;7:442–53.
[198] Zhao J, Zhang X, Yonzon CR, Haes AJ, Van Duyne RP. Localized surface plasmon resonance biosensors. Nanomedicine 2006;1:219–28.
[199] Sun Y, Xia Y. Increased sensitivity of surface plasmon resonance of gold nanoshells compared to that of gold solid colloids in response to environmental changes. Anal Chem 2002;74:5297–305.
[200] Fleischmann M, Hendra PJ, McQuillan AJ. Raman spectra of pyridine adsorbed at a silver electrode. Chem Phys Lett 1974;26:163–6.
[201] Jeanmaire DL, Van Duyne RP. Surface Raman spectroelectrochemistry Part I. Heterocyclic, aromatic, and aliphatic amines adsorbed on the anodized silver electrode. J Electroanal Chem Interfacial Electrochem 1977;84:1–20.
[202] Albrecht MG, Creighton JA. Anomalously intense Raman spectra of pyridine at a silver electrode. J Am Chem Soc 1977;99:5215–17.
[203] Stiles PL, Dieringer JA, Shah NC, Van Duyne RP. Surface-enhanced Raman spectroscopy. Annu Rev Anal Chem 2008;1:601–26.
[204] Nie S, Emory SR. Probing single molecules and single nanoparticles by surface-enhanced Raman scattering. Science 1997;275:1102–6.
[205] Kneipp K, Wang Y, Kneipp H, Perelman LT, Itzkan I, Dasari RR. Feld MS. Single molecule detection using surface-enhanced Raman scattering (SERS). Phys Rev Lett 1997;78:1667–70.
[206] Michaels AM, Nirmal M, Brus LE. Surface enhanced Raman spectroscopy of individual rhodamine 6G molecule on large Ag nanocrystals. J Am Chem Soc 1999;121:9932–9.
[207] Xu HX, Bjerneld EJ, Kall M, Borjesson L. Spectroscopy of single haemoglobin molecules by surface enhanced Raman scattering. Phys Rev Lett 1999;83:4357–60.
[208] Blackie EJ, Le Ru EC, Etchegoin PG. Single-molecule surface-enhanced Raman spectroscopy of nonresonant molecules. J Am Chem Soc 2009;131:14466–72.
[209] Mirsaleh-Kohan N, Iberi V, Simmons PD, Bigelow NW, Vaschillo A, Rowland MM, Best MD, Pennycook SJ, Masiello DJ, Guiton BS, Camden JP. Single-molecule surface-enhanced Raman scattering: can STEM/EELS image electromagnetic hot spots? J Phys Chem Lett 2012;3:2303–9.
[210] Qian X, Peng XH, Ansari DO, Yin-Goen Q, Chen GZ, Shin DM, Yang L, Young AN, Wang MD, Nie S. In vivo tumor targeting and spectroscopic detection with surface-enhanced Raman nanoparticle tags. Nature Biotech 2008;26:83–90.
[211] Maher RC, Maier SA, Cohen LF, Koh L, Laromaine A, Dick JAG, Stevens MM. Exploiting SERS hot spots for disease-specific enzyme detection. J Phys Chem C 2010;114:7231–5.
[212] Xu L, Yan W, Ma W, Kuang H, Wu X, Liu L, Zhao Y, Wang L, Xu C. SERS encoded silver pyramids for attomolar detection of multiplexed disease biomarkers. Adv Mater 2015;27:1706–11.
[213] Lee S, Chon H, Lee M, Choo J, Shin SY, Lee YH, Rhyu IJ, Son SW, Oh CH. Surface-enhanced Raman scattering imaging of HER2 cancer markers overexpressed in single MCF7 cells using antibody conjugated hollow gold nanospheres. Biosens Bioelectron 2009;24:2260–3.
[214] Laurence TA, Braun G, Talley C, Schwartzberg A, Moskovits M, Reich N, Huser T. Rapid, solution-based characterization of optimized SERS nanoparticle substrates. J Am Chem Soc 2009;131:162–9.
[215] Gao L, Liu R, Gao F, Wang Y, Jiang X, Gao X. Plasmon-mediated generation of reactive oxygen species from near-infrared light excited gold nanocages for photodynamic therapy in vitro. ACS Nano 2014;8:7260–71.
[216] Govorov AO, Richardson HH. Generating heat with metal nanoparticles. Nano Today 2007;2:30–8.
[217] Jin Y. Engineering plasmonic gold nanostructures and metamaterials for biosensing and nanomedicine. Adv Mater 2012;24:5153–65.
[218] Khlebtsov BN, Panfilova EV, Terentyuk GS, Maksimova IL, Ivanov AV, Khlebtsov NG. Plasmonic nanopowders for photothermal therapy of tumors. Langmuir 2012;8:8994–9002.
[219] Donner JS, Thompson SA, Alonso-Ortega C, Morales J, Rico LG, Santos SI, Quidant R. Imaging of plasmonic heating in a living organism. ACS Nano 2013;10:8666–72.
[220] Xiong W, Mazid R, Yap LW, Li X, Cheng W. Plasmonic caged gold nanorods for near-infrared light controlled drug delivery. Nanoscale 2014;6:14388–93.
[221] Patino T, Mahajan U, Palankar R, Medvedev N, Walowski J, Münzenberg M, Mayerle J, Delcea M. Multifunctional gold nanorods for selective plasmonic photothermal therapy in pancreatic cancer cells using ultra-short pulse near-infrared laser irradiation. Nanoscale 2015;7:5328–37.
[222] You J, Zhang G, Li C. Exceptionally high payload of doxorubicin in hollow gold nanospheres for near-infrared light-triggered drug release. ACS Nano 2010;4:1033–41.
[223] Skrabalak SE, Chen J, Au L, Lu X, Li X, Xia Y. Gold nanocages for biomedical applications. Adv Mater 2007;19:3177–84.
[224] Melancon MP, Lu W, Yang Z, Zhang R, Cheng Z, Elliot AM, Stafford J, Olson T, Zhang JZ, Li C. In vitro and in vivo targeting of hollow gold nanoshells directed at epidermal growth factor receptor for photothermal ablation therapy. Mol Cancer Ther 2008;7:1730–9.
[225] Lu W, Xiong C, Zhang G, Huang Q, Zhang R, Zhang JZ, Li C. Targeted photothermal ablation of murine melanomas with melanocyte-stimulating hormone analog-conjugated hollow gold nanospheres. Clin Cancer Res 2009;15:876–86.
[226] Chithrani BD, Ghazani AA, Chan WCW. Determining the size and shape dependence of gold nanoparticle uptake into mammalian cells. Nano Lett 2006;6:662–8.

Brought to you by | Hospital Universitari Vall d'Hebron
Authenticated
Download Date | 3/7/19 12:30 PM

[227] Boisselier E, Astruc D. Gold nanoparticles in nanomedicine: preparations, imaging, diagnostics, therapies and toxicity. Chem Soc Rev 2009;38:1759–82.
[228] Mahmoud MA, Saira F, El-Sayed MA. Experimental evidence for the nanocage effect in catalysis with hollow nanoparticles. Nano Lett 2010;10:3764–9.
[229] Slater TJA, Macedo A, Schroeder SLM, Burke MG, O'Brien P, Camargo PH, Haigh SJ. Correlating catalytic activity of Ag-Au nanoparticles with 3D compositional variations. Nano Lett 2014;14:1921–6.
[230] Mahmoud MA, Narayanan R, El-Sayed M. Enhancing colloidal metallic nanocatalysis: sharp edges and corners for solid nanoparticles and cage effect for hollow ones. Acc Chem Res 2013;46:1795–805.
[231] Zeng J, Zhang Q, Chen J, Xia Y. A comparison study of the catalytic properties of Au-based nanocages, nanoboxes, and nanoparticles. Nano Lett 2010;10:30–5.
[232] Wu H, Wang P, He H, Jin Y. Controlled synthesis of porous Ag/Au bimetallic hollow nanoshells with tunable plasmonic and catalytic properties. Nano Res 2012;5:135–44.

Brought to you by | Hospital Universitari Vall d'Hebron
Authenticated
Download Date | 3/7/19 12:30 PM